

Predictive control and modeling of a point absorber wave energy harvesting connected to the grid using a LPMSG-based power converter

Abderrahmane Berkani¹, Mofareh Hassan Ghazwani², Karim Negadi¹,
Lazreg Hadji^{*3}, Ali Alnujaie² and Hassan Ali Ghazwani²

¹L2GEGI Laboratory, Department of Electrical Engineering, Faculty of Applied Science, University of Tiaret, BP 78 Zaaroura, 14000, Tiaret, Algeria

²Department of Mechanical Engineering, Faculty of Engineering, Jazan University, P.O. Box 114, Jazan, 45142, Kingdom of Saudi Arabia

³Department of Civil Engineering, University of Tiaret, BP 78 Zaaroura, Tiaret, 4000, Algeria

(Received July 2, 2023, Revised January 13, 2024, Accepted January 14, 2024)

Abstract. In this paper, the authors explore the modeling and control of a point absorber wave energy converter, which is connected to the electric grid via a power converter that is based on a linear permanent magnet synchronous generator (LPMSG). The device utilizes a buoyant mechanism to convert the energy of ocean waves into electrical power, and the LPMSG-based power converter is utilized to change the variable frequency and voltage output from the wave energy converter to a fixed frequency and voltage suitable for the electric grid. The article concentrates on the creation of a predictive control system that regulates the speed, voltage, and current of the LPMSG, and the modeling of the system to simulate its behavior and optimize its design. The predictive model control is created to guarantee maximum energy output and stable grid connection, using Matlab Simulink to validate the proposed strategy, including control side generator and predictive current grid-side converter loops.

Keywords: back to back converter; LPMSG; multi-level inverter; point absorber; predictive control; wave energy harvesting

1. Introduction

The use of renewable energy sources has gained significant attention in recent years due to the need to reduce greenhouse gas emissions and mitigate the effects of climate change (Richter 2011). One promising source of renewable energy is ocean waves, which contain a significant amount of energy that can be harnessed and converted into electricity using wave energy converters. Point absorber wave energy converters are a type of wave energy converter that uses a buoyant device to capture the energy of ocean waves (Xu *et al.* 2020). To connect the point absorber wave energy converter to the electric grid, a power converter based on a linear permanent magnet synchronous generator (LPMSG) can be used. However, to ensure optimal energy output and a stable grid

*Corresponding author, Professor, E-mail: lazreg.hadji@univ-tiaret.dz; had_laz@yahoo.fr

connection, a control system must be developed to regulate the speed, voltage, and current of the LPMSG. This article focuses on the modeling and control of a point absorber wave energy converter connected to the electric grid using a PMSG-based power converter (Richter *et al.* 2013, Huang *et al.* 2021). The article presents mathematical models of the system and control strategies, such as maximum power point tracking and voltage control loops that can be used to optimize the system design and improve its performance.

The point absorber technique is a method for capturing energy from ocean waves, which dates back to the early 20th century. The concept of using buoys or other floating devices to extract energy from ocean waves was first proposed by French mathematician and physicist Pierre-Simon Laplace in 1779.

However, it wasn't until the 1930s that the first practical wave energy devices based on the point absorber principle were developed (Aguirre *et al.* 2021). One of the earliest examples was the Salter Duck, invented by Scottish engineer Stephen Salter in the 1970s. The Salter Duck was a floating device that used a wave-activated hydraulic pump to generate electricity.

In the decades that followed, numerous other point absorber devices were developed, each with its own unique design and operating principle. One example is the Power Buoy, developed by Ocean Power Technologies in the 1990s. The Power Buoy is a buoyant cylinder that is anchored to the ocean floor and uses the motion of the waves to drive a generator (Srivastava and Bajpai 2022).

Another example is the Wave roller, developed by AW-Energy in the early 2000s. The Wave roller is a large, articulated panel that is attached to the ocean floor and uses the motion of the waves to generate electricity.

Today, the point absorber technique remains a popular method for generating electricity from ocean waves, with numerous commercial-scale devices in operation around the world (Shengquan *et al.* 2020). While there are still technical and economic challenges to be addressed, ongoing research and development are helping to improve the efficiency and reliability of point absorber wave energy devices (Babes *et al.* 2017).

Predictive control is a powerful technique used in various control applications, including renewable energy systems. In the case of wave energy converters, the aim is to extract as much energy as possible from ocean waves to generate electrical power. This involves controlling the power take-off system, which is typically made up of a permanent magnet synchronous generator (PMSG) or a linear permanent magnet synchronous generator (LPMSG).

PMSGs and LPMSGs are commonly used in wave energy converters due to their high efficiency and reliability (Makhad *et al.* 2020). However, their performance can be greatly enhanced by using predictive control techniques. Predictive control involves predicting the future behavior of a system based on its current state and using this information to determine the optimal control actions to achieve a desired outcome (Amon *et al.* 2012, Hung and Nguyễn).

In the case of wave energy converters, predictive control can be used to optimize the power take-off system by predicting the wave conditions and adjusting the control actions of the generator accordingly. This approach allows for improved energy capture and increased efficiency, ultimately leading to higher power output and better performance (Artal-Sevil *et al.* 2018, Duthoit and Falzarano 2018, Adaryani *et al.* 2020, Poguluri *et al.* 2022).

Overall, the use of predictive control in PMSG and LPMSG-based wave energy converters is a promising area of research that has the potential to greatly improve the efficiency and effectiveness of these renewable energy systems (Eedara *et al.* 2019).

The paper is structured as follows. Firstly, the introduction provides a brief overview of the case study. Secondly, section 2 describe of the marine conversion using a point absorber process. Section

3 gives the electrical consideration of a wave energy based a pint absorber. The physical modeling of the different components in the setup is the object of section 4. In section 5 and 6, predictive model control-based power generation is presented. Section 7 presents the simulation results and analysis. Lastly, section 8 summarizes the main findings of the research and discusses potential future developments.

2. Description of a marine conversion chain based point absorber process

A point absorber wave energy converter is a device that converts wave energy into electricity using a buoyant device that moves up and down with the waves, driving a power take-off system. The power take-off system is typically a linear generator or a hydraulic pump that drives a hydraulic motor or an electric generator, which converts the mechanical energy into electrical energy (Berkani *et al.* 2020).

To connect the point absorber wave energy converter to the electric grid, a power converter based on a permanent magnet synchronous generator (PMSG) can be used. The power converter converts the variable frequency and voltage output from the wave energy converter to a fixed frequency and voltage that is suitable for the electric grid.

To model and control the point absorber wave energy converter connected to the electric grid via a power converter based on a PMSG, a control system must be designed to regulate the generator speed, voltage, and current. The control system should ensure that the generator operates at the optimal speed and voltage to maximize the energy output and maintain a stable grid connection (Josset *et al.* 2007).

One common control strategy for wave energy converters is the maximum power point tracking (MPPT) algorithm, which adjusts the generator speed to maximize the energy output. The MPPT algorithm can be combined with a voltage control loop to regulate the generator voltage and ensure a stable grid connection.

To model the wave energy converter and power converter system, mathematical models can be developed based on the equations of motion for the buoyant device and the electrical equations for the generator and power converter. These models can be used to simulate the system behavior and optimize the control system design.

Overall, the modeling and control of a point absorber wave energy converter connected to the electric grid via a power converter based on a PMSG involves a multidisciplinary approach that combines mechanical, electrical, and control engineering principles.

3. Electrical considerations for Wave Energy Converters (WECs)

The transfer of energy in waves occurs at the wave group velocity, typically between 5 and 10 m/s (Casagrande 2015). This variation in frequency leads to fluctuations in the power captured by the absorber, causing the electrical generator to operate in a pulsating pattern and generate voltages and currents that vary with time, as illustrated in Fig. 1. Power electronic converters are therefore necessary to stabilize this fluctuating power output and make it constant over time, making it suitable for connection to the utility grid (Yemane 2019). The pulsating nature of the power becomes even more significant when the WEC system is connected to a weak grid, which is common in remote areas with high wave activity. The harsh environmental conditions, including humidity, corrosion,

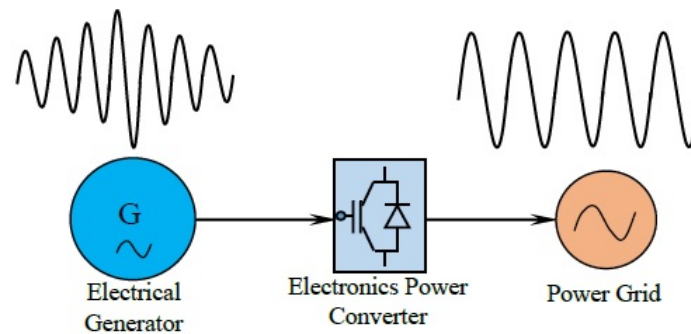


Fig. 1 Electrical power conversion based WEC

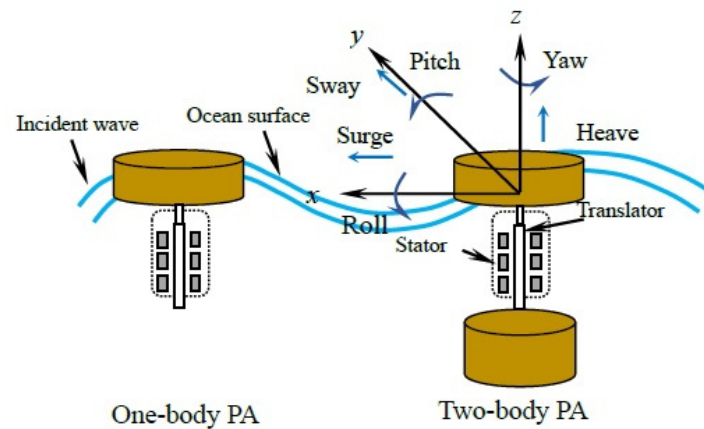


Fig. 2 Constitution of the process point absorber (Wong and Yi 2018)

vibrations, and mechanical stresses caused by the pulsating pattern, pose a challenge for the design of power electronic converters in WECs (Faizal *et al.* 2014). Multipole generators with direct-drive controllers are recommended due to their improved reliability. Energy storage systems (ESSs), such as flywheel mechanisms, batteries, and super-capacitors, can help to smooth the generated power and improve the system's performance when connected to weak grids, particularly during off-peak periods (Sun *et al.* 2020).

To maximize power harvesting from WEC systems, the phase of the device's speed divided by the phase of the wave's excitation force should be adjusted to a specific value (Ruezga *et al.* 2021), which requires bidirectional power flow between the converter's input and output, which can be further improved by using ESSs. However, this process can be complicated and may result in large currents and voltages that could damage the converter.

Modeling of a point absorber is an important aspect of designing and optimizing wave energy converters (WECs) that harness energy from ocean waves. A point absorber is a type of WEC that consists of a buoy that moves up and down with the motion of the waves, driving a power take-off system that generates electricity (see Fig. 2).

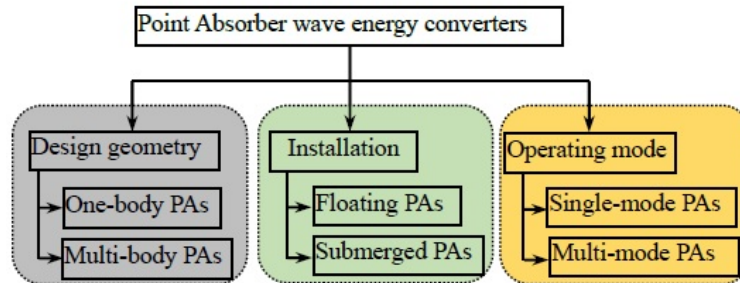


Fig. 3 Classification of point absorber wave energy converters

The modeling of a point absorber involves creating mathematical equations that describe the motion of the buoy and the energy conversion process. The buoy motion is typically modeled using linear wave theory, which assumes that the waves are small and that the motion of the buoy is simple harmonic motion. The power take-off system can be modeled using various techniques, including lumped parameter models, finite element models, and system identification techniques (Anderlini *et al.* 2018).

The modeling of a point absorber is important for several reasons. First, it allows designers to optimize the WEC for maximum energy conversion efficiency. Second, it provides a means to predict the performance of the WEC under different wave conditions, which is important for assessing the economic viability of the system. Third, it allows researchers to study the dynamic behavior of the WEC and to develop control strategies to improve its performance (Backer 2009).

Overall, the modeling of a point absorber is an essential step in the design and optimization of wave energy converters, and it plays a critical role in the development of this emerging renewable energy technology.

3.1 Point absorber categorization

Fig. 4 illustrates that PAs can be categorized based on - Their design geometry as either one-body or multi-body Pas (Ghany *et al.* 2021).

- Their deployment method as either floating or submerged devices.
- Their operating degrees of freedom as either single-DoF or multi-DoF prototypes.

The categorization of point absorbers depends on various factors such as the geometry, design, and operation of the device, as well as the specific characteristics of the waves at the installation site.

In this paper, we will adopt the geometry-based one body PA with a floating operate at single mode.

3.2. Point absorber (Buoy)

The operation of a buoy in the ocean is straightforward. Wind energy transfers onto the ocean surface, generating waves. Strong winds blowing over long distances result in large waves. The buoy floats on the surface, moving up with a wave crest and down with a wave trough. This mechanical

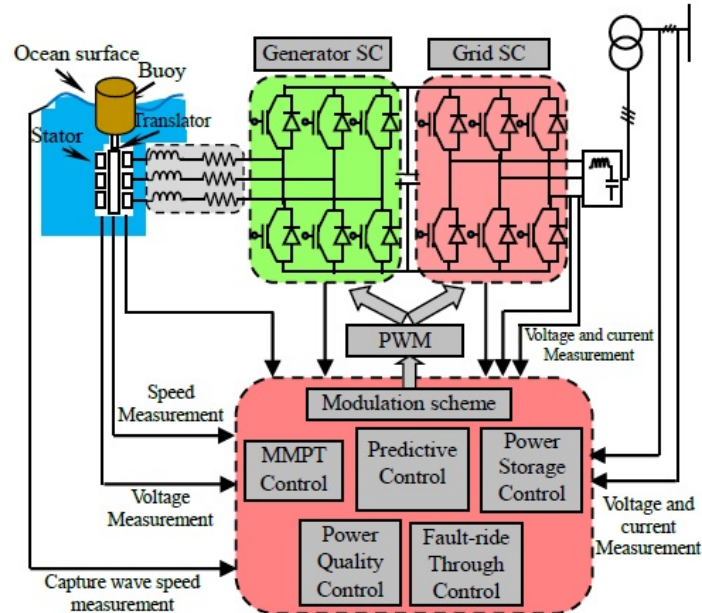


Fig. 4 General control structure of ocean energy system based point absorber and LPMSG

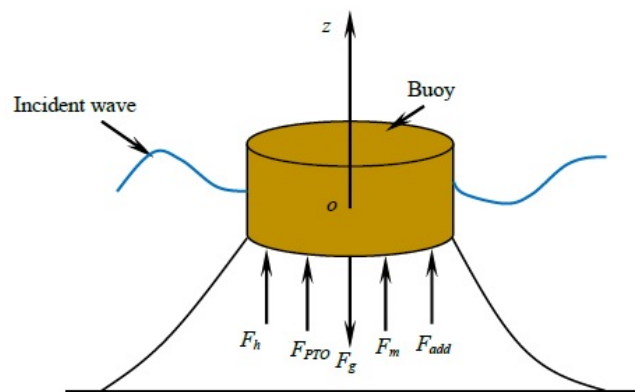


Fig. 5 A floating cylindrical buoy is used to illustrate the dynamics of a generic PA device

movement caused by the waves generates energy that can be used to drive an electric generator. Additionally, the wave energy can be transmitted to the shore through an underwater power cable and connected to the utility grid. An example of a WEC device, the PB40 Power Buoy wave energy converter prototype (Fabrizio *et al.* 2015).

The diagram in Fig. 5 depicts a point absorber wave energy converter (WEC) with a direct drive linear generator and a back-to-back converter system linked to the grid. The rectifier is responsible for regulating the reaction force generated to optimize the capture of power from sea waves. Meanwhile, the inverter maintains a constant voltage on the DC link.

Table 1 The technical characteristics associated with the buoy model

Model	Geometry			Mass	Water depth
	Diameter	Height	Area		
Buoy	4 m	1 m	36.201 m ²	6700 kg	50 m

The geometric dimensions of a point absorber buoy can vary depending on its specific design and intended use, but some common dimensions include:

- Buoy diameter: This refers to the width of the buoy, which can range from a few meters to tens of meters.
- Draft: This refers to the depth of the buoy below the waterline, which can also vary depending on the design.
- Stroke length: This refers to the distance that the buoy travels up and down with each passing wave, which can range from a few meters to tens of meters.
- Tether length: This refers to the length of the tether that connects the buoy to the seabed, which can be several times the water depth.
- Height above water: This refers to the distance from the waterline to the top of the buoy, which can vary depending on the specific design and intended use.

Table 1 outlines the technical parameters, such as mass, diameter, area, and others, of the proposed point absorber model (Li and Yu 2012).

The geometric dimensions of a point absorber buoy are critical factors that influence its performance and efficiency in converting wave energy into electricity.

4. Advanced modelling of WEC based PA

This section provides a fundamental understanding of Wave Energy Converters (WECs). It explains the wave equation and the different forces that impact the wave equation, ultimately shaping the motion of the point absorbers.

The study assumes that waves are mono-directional and propagate in the positive x-direction. The system is axis-symmetric, and all motions occur in the (x0z) plane. The point absorber interacts with the ocean primarily in the Surge, Heave, and Pitch directions, with Heave being the most efficient mode for wave energy extraction. The point absorber is modeled with one degree of freedom, Heave, using Newton's second law (Tagliafierro *et al.* 2022)

$$F_{pe}(t) + F_{re}(t) = m\ddot{z}(t) \quad (1)$$

In traditional point absorber modeling, the primary forces considered are:

m : which represents the overall inertia of the system,

z : representing its heave displacement (in the vertical direction).

F_{pe} : the external pressure-induced force (such as hydrodynamic or hydrostatic).

F_{re} : the reaction force that encompasses the loads associated with the PTO and mooring foundation.

Referring to Newton's second law (Zhang *et al.* 2022)

$$F_E(t) + F_{PTO}(t) = m\ddot{z}(t) + F_R(t) + F_B(t) + F_v(t) + F_l(t) + F_o(t) \quad (2)$$

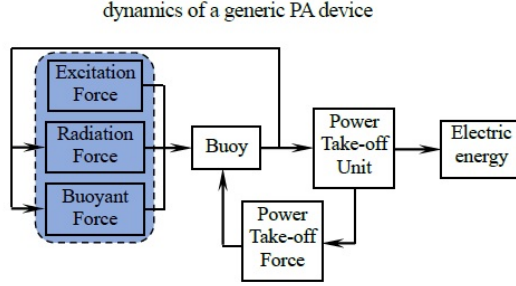


Fig. 6 Force applied to the heave axis of a point absorber

The equation involves several forces acting on the system, including the mass of the buoy (m), radiation force (F_{Rad}), buoyancy force (F_B), viscous force (F_v), mooring force (F_l), environmental force (F_o), wave excitation force (F_E), and Power Take Off (PTO) force (F_{PTO}).

For this study, we will only consider linear terms, which is typical for this application. As a result, the viscous, mooring, and environmental forces will not be taken into account. The resulting equation is

$$F_E(t) + F_{PTO}(t) = m\ddot{z}(t) + F_R(t) + F_B(t) \quad (3)$$

Based on the assumption of linear hydrodynamics (Engin and Yeşildirek 2015), Eq. (3) can be expressed in the frequency domain as (Muljadi *et al.* 2015).

$$F_E(\omega) + F_{PTO}(\omega) = -m\omega^2 z(\omega) + F_R(\omega) + F_B(\omega) \quad (4)$$

The primary forces generally considered in the conventional modeling of point absorbers are represented in Fig. 5 and the relationship that exists between the different forces and the electrical energy delivered by the point absorber is shown in Fig. 6.

4.1 The force of radiation

The expression for the radiation force is given by (Xu and Li 2011)

$$F_R(\omega) = m_r(\omega)a(\omega) + R_r(\omega)v(\omega) \quad (5)$$

The equation includes several parameters, where $m_r(\omega)$ represents the added mass that varies with frequency due to the near-field standing wave, and $R_r(\omega)$ represents the radiation resistance associated with outgoing waves in the far-field. The parameters $u(\omega)$ and $a(\omega)$ correspond to the speed and acceleration in the frequency domain, respectively. Specifically, $a(\omega)$ equals $-\omega^2 z(\omega)$, and $v(\omega)$ is given by $j\omega z(\omega)$.

It is possible to linearize the radiation force (Guo *et al.* 2022) and represent it in the time domain as follows

$$F_R(t) = m_r(\infty)\ddot{z} + \int_0^t H_{rad}(t-\tau)\dot{z}(\tau)d\tau \quad (6)$$

The radiation parameters in equation (6) can be estimated using constant coefficients, as proposed in (Annalisse *et al.* 2014).

$$F_R(t) = -A\ddot{z}(t) - B\dot{z}(t) \quad (7)$$

This can be represented in the frequency domain as

$$F_R(\omega) = (\omega^2 A - j\omega B)z(\omega) \quad (8)$$

4.2 Excitation force

To calculate the excitation force, one needs to multiply the elevation η by the excitation force coefficient h_η (Liguo *et al.* 2017). The value of h_η is influenced by the object's geometry. In order to represent the excitation force over time, the following expression can be used (El-Shalakany *et al.* 2022):

The excitation force acts on the buoy due to incident waves and it does not depend on the buoy motion.

$$F_E(t) = h_\eta(t)\eta_{ref}(t) \quad (9)$$

Described in the frequency domain

$$F_E(\omega) = H_\eta(\omega)\eta_{ref}(\omega) \quad (10)$$

To compute the excitation force using Eq. (10), the incident wave's elevation is taken as an input. Alternatively, one could assume the excitation force as the input and use a linearized Morison approach to calculate it (Michael *et al.* 2014).

$$F_E(t) = A\ddot{\eta}(t) + B\dot{\eta}(t) + k\eta(t) \quad (11)$$

In this equation, A represents the added mass, B represents the radiation damping, and k represents the hydrostatic stiffness.

4.3 The float buoyancy force

The expression for the buoyancy force is given by

$$F_B(t) = g\rho A_\omega z(t) = g\rho\pi r_{float}^2 z(t) \quad (12)$$

The equation includes several parameters, such as A_ω , which represents the water surface area of the point absorber. It is typically assumed to be circular, as illustrated in Fig. 5. Other parameters include g , which corresponds to gravity, and ρ , which represents the density of water.

4.4 Power Take Off (PTO)

The Power Take-Off (PTO) system is responsible for converting the absorbed buoyancy energy of the point absorber into electrical energy. The PTO system can impact several aspects of the wave energy converter, such as the amount of absorbed wave energy, as well as the size, mass, and structural dynamics of the device (Noman *et al.* 2021, Hung and Nguyen 2022). Different types of PTO systems can be employed in point absorbers, including cascaded conversion mechanisms.

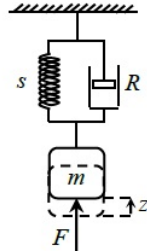


Fig. 7 A Point absorber represented by a mass-spring-damper system as a mechanical oscillator

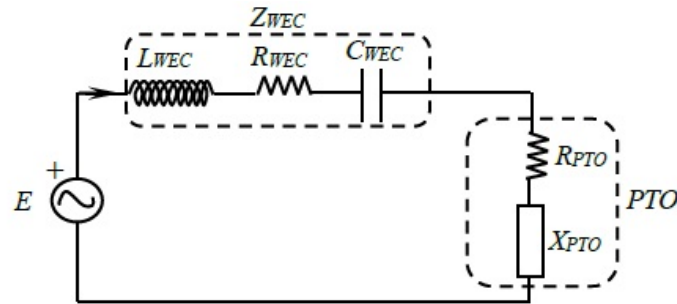


Fig. 8 Point Absorber Wave Energy Converter Electric Circuit

The linear model of the Power Take-Off (PTO) system can be expressed as

$$F_{PTO}(t) = -B_{PTO}\dot{z}(t) - M_{PTO}\ddot{z}(t) - S_{PTO}z(t) \quad (13)$$

The equation for the linear model of the Power Take-Off (PTO) system includes various coefficients, such as B_{PTO} for the damping coefficient, M_{PTO} for the spring coefficient, and S_{PTO} for the stiffness coefficient.

The Mass-Spring-Damper (MSD) system is a widely used model for describing the dynamics of wave energy converters (WECs). In free oscillation, the MSD system can be used to predict the natural frequency and damping ratio of the WEC. The electric analogue of the MSD system can be used to design and optimize the power take-off (PTO) system of the WEC, which converts the absorbed wave energy into electrical power.

5. Dynamic model of electrical part of wave energy conversion

5.1 The model of LPMSG

Linear Permanent Magnet Generators The linear permanent magnet generator (LPMG) consists of a set of magnets mounted on the translator oscillating within the stator, made up of the yoke, teeth and the three phase cylindrically distributed coil windings. Fig. 2 shows the configuration of the

LPMSG and the paths of magnetic flux between the translator (also referred to as the actuator) and the stator. The flux is shown to cross the air gap from the magnets in the translator through the stator tooth, bifurcating in the stator yoke and returning back to the translator from the adjacent magnet. Danielsson (Pastor *et al.* 2014) provides more details about the windings, magnets and stator characteristics.

LPMGs offer several advantages, such as relatively high efficiency, which has been reported to be over 86% (Giralda *et al.* 2021), and the possibility of continuous force control. However, there are also notable drawbacks, including the low power to weight ratio, which requires the use of very large machines, and the need for a heavy structure due to the attractive forces between the stator and translator. To address these issues, air-cored/iron-less configurations have been proposed (Ghany *et al.* 2021), which can significantly reduce the weight of the structure and the magnetic force.

The dynamics of linear electric generators are similar to those of rotary electric generators.

The equations describing the stator voltage of the LPMSG in the abc reference frame can be expressed in the following manner

$$\begin{bmatrix} v_a \\ v_b \\ v_c \end{bmatrix} = -R_s \begin{bmatrix} i_a \\ i_b \\ i_c \end{bmatrix} - L_s \frac{d}{dt} \begin{bmatrix} i_a \\ i_b \\ i_c \end{bmatrix} + \omega_e \Psi_{PM} \begin{bmatrix} \cos \theta \\ \cos \left(\theta - \frac{2\pi}{3} \right) \\ \cos \left(\theta - \frac{4\pi}{3} \right) \end{bmatrix} \quad (14)$$

Where:

v_a, v_b and v_c : are the individual voltages across the stator windings.

i_a, i_b and i_c : are the currents flowing into the stator windings

R_s : is the equivalent resistance of each stator winding.

Ψ_{pm} : the permanent magnet flux,

ω_e : is the electromechanical speed of the generator.

However, the equations used to describe rotary generators must be adapted to account for the linear motion of the rotor. The dynamics of LPMGs can be expressed as follows (Adaryani *et al.* 2021)

$$\begin{cases} v_{sd} = -R_s i_{sd} - L_d \frac{di_{sd}}{dt} + L_q \omega_e i_{sq} \\ v_{sq} = -R_s i_{sq} - L_q \frac{di_{sq}}{dt} - L_d \omega_e i_{sd} + \omega_e \Psi_{PM} \end{cases} \quad (15)$$

where:

L_d : is d-axis inductance,

L_q : is q-axis inductance

v_{sd}, v_{sq} are stator voltage components in d-q reference frame.

i_{sd}, i_{sq} are stator current components in d-q reference frame.

In the Simulink model, the permanent magnet synchronous machine block operates as a generator when the torque and angular velocity have opposite signs, and as a motor when they have the same sign. Thus, the 'motor convention' is employed, whereby the torque sign is inverted to utilize the machine as a generator. Eqs. (15) in the 'motor convention' are equivalent to

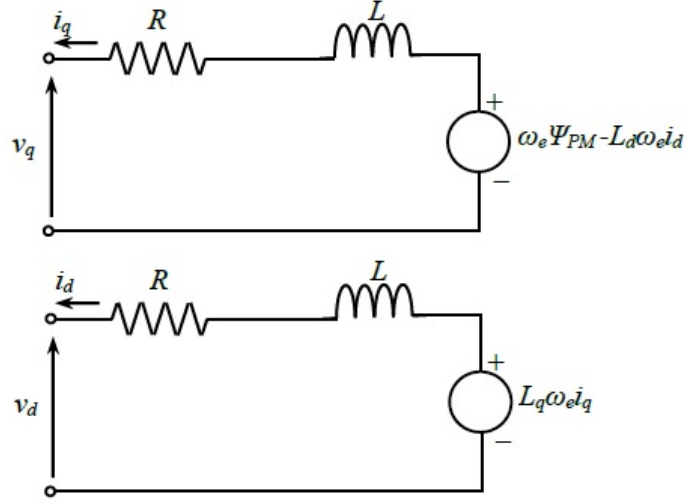


Fig. 9 Generator Circuit Equivalent in d and q Axes

$$\begin{cases} v_{sd} = +R_s i_{sd} + L_d \frac{di_{sd}}{dt} - L_q \omega_e i_{sq} \\ v_{sq} = +R_s i_{sq} + L_q \frac{di_{sq}}{dt} + L_d \omega_e i_{sd} + \omega_e \Psi_{PM} \end{cases} \quad (16)$$

The figure below displays the d and q axis circuits of the generator's equivalent, utilizing the conventions outlined in Eq. (15).

The resulting electromagnetic torque of the generator is expressed in dq frame of reference as

$$T_{em} = \frac{3}{2} p (\Psi_{PM} + (L_d - L_q) i_{sd}) i_{sq} \quad (17)$$

According to Eq. (18), it is demonstrated that the generator's torque can be controlled directly by the i_q parameter (Yaramasu et al. 2017)

$$T_{em} = \frac{3}{2} p \Psi_{PM} i_{sq} \quad (18)$$

$$T_{em} = \frac{3}{2} p \Psi_{PM} i_{sq} \quad (19)$$

Where:

p : is the number of pole pairs.

The mechanical behavior is characterized by the following dynamics

$$J \frac{d\omega_m}{dt} = T_T - T_{em} \quad (20)$$

J denotes the moment of inertia of the rotating components, T_T represents the torque of the turbine and T_{em} is the torque of the generator.

The expression for the active power of an LPMSG is as follows

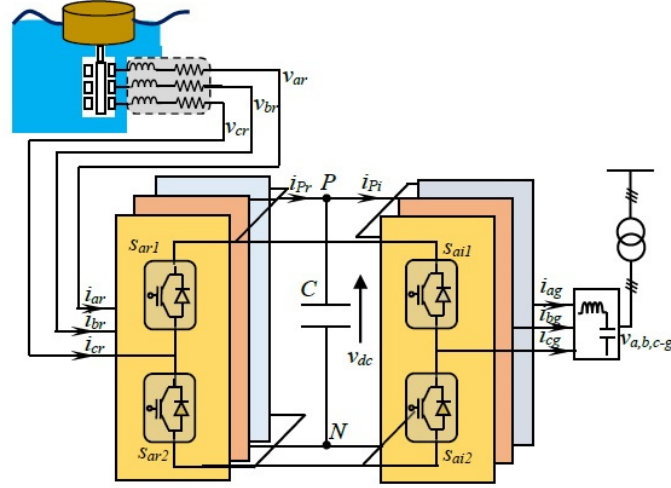


Fig. 10 WEC based PA using Back-to-Back 2L Voltage Source Converters

$$P = \frac{3}{2} \psi_{PM} \omega_e i_{sq} \quad (21)$$

The maximum active power that can be generated by each PMSG is

$$P = \frac{3}{2} \psi_{PM} \frac{V_{lim}}{L_q} \quad (22)$$

The constant values of ψ_{PM} and L_q imply that the voltage limit is a determining factor for the maximum active power. By substituting V_{lim} , L_q , and ψ_{PM} into the equation, the maximum active power that can be produced by each LPMSG is nearly a hundred kilowatts.

5.2 Design of a back-to-back converter for point absorber application

A back-to-back converter with a linear permanent magnet synchronous generator (LPMSG) is a promising solution for point absorber wave energy converter (WEC) applications. To model and design this type of converter, several factors must be considered (Pranupa *et al.* 2022).

Firstly, the electrical and mechanical characteristics of the PMSG must be determined. This includes the electrical parameters such as the inductance and resistance, as well as the mechanical parameters such as the damping coefficient and natural frequency.

Next, the back-to-back converter topology must be designed to regulate the power flow between the WEC and the grid, and to control the rotational speed of the LPMSG. This involves selecting appropriate switching devices, designing the control system, and determining the necessary feedback signals.

Finally, the system must be simulated and tested to validate the design and ensure that it meets the performance requirements. This includes conducting simulations to evaluate the efficiency, stability, and dynamic response of the system under various operating conditions.

Overall, the use of a back-to-back converter with a linear PMSG has the potential to improve the efficiency and reduce the cost of energy production for point absorber WEC applications, making it a promising solution for renewable energy generation (Lee *et al.* 2014).

The back-to-back (BTB) configuration illustrated in Fig. 10 can be modeled using the same approach as other types of power converters. In this configuration, the two-level voltage source rectifier (2L-VSR) and two-level voltage source inverter (2L-VSI) are connected via a DC-link capacitor.

Variables on the rectifier and inverter sides are differentiated by subscripts r and i, respectively. The output voltages for each phase of the converter (denoted as x , where $x \in \{a, b, c\}$) are referenced to the negative DC-bus N and labeled as v_{xr} and v_{xi} . Similarly, the line currents for the rectifier and inverter are labeled as i_{xr} and i_{xi} , respectively.

The computation of the output voltages for the two-level voltage source rectifier and the two-level voltage source inverter can be represented as

$$\begin{bmatrix} v_{ar} \\ v_{br} \\ v_{cr} \end{bmatrix} = v_{dc} \begin{bmatrix} S_{ar1} \\ S_{br1} \\ S_{cr1} \end{bmatrix}, \quad \begin{bmatrix} v_{ag} \\ v_{bg} \\ v_{cg} \end{bmatrix} = v_{dc} \begin{bmatrix} S_{ai1} \\ S_{bi1} \\ S_{ci1} \end{bmatrix} \quad (23)$$

Currently, there is a utilization of an electric current estimation (i_{c1}) that flows through the DC link capacitor C (Jingjin and Lei 2013):

$$\begin{aligned} i_{c1} &= i_{Pr} - i_{Pi} \\ &= (S_{ar1}i_{ar} + S_{br1}i_{br} + S_{cr1}i_{cr}) - (S_{as1}i_{ag} + S_{bs1}i_{bg} + S_{cs1}i_{cg}) \end{aligned} \quad (24)$$

The active and reactive powers of the stator are represented in watts (W) and volt-amperes reactive (VAR) units, respectively

$$\begin{cases} P_s = \frac{3}{2}(v_{ds}i_{ds} + v_{qs}i_{qs}) \\ Q_s = \frac{3}{2}(v_{qs}i_{ds} - v_{ds}i_{qs}) \end{cases} \quad (25)$$

The GSC, grid filter, and DC bus are specifically created to regulate the DC-link voltage by producing or absorbing reactive power. Their purpose is to maintain a consistent and stable DC voltage.

The allocation of active and reactive power between the grid and the grid-side converter (GSC) is decided based on their individual units of measurement. The GSC is measured in watts (W), while the grid is measured in volt-amperes reactive (VAR).

$$\begin{cases} P_g = \frac{3}{2}(v_{dg}i_{dg} + v_{qg}i_{qg}) \\ Q_g = \frac{3}{2}(v_{qg}i_{dg} - v_{dg}i_{qg}) \end{cases} \quad (26)$$

where:

v_{dg} and v_{qg} : are the d-q grid voltage (V),

i_{dg} and i_{qg} : are the d-q grid currents (A).

6. Purpose of predictive control

Integrating predictive control into a wave energy conversion system based on a point absorber can offer several advantages, such as:

- Improved energy capture: predictive control algorithms can optimize the motion of the point absorber based on wave conditions, resulting in improved energy capture and higher efficiency (Singh 2020).

- Reduced stress on components: predictive control can help reduce the stress on components by adjusting the motion of the point absorber to minimize excessive motion or loading. This can help prolong the lifespan of the system and reduce maintenance costs.

- Increased reliability: predictive control algorithms can monitor the performance of the wave energy conversion system and automatically take corrective action if necessary. This can help prevent system failures and improve the reliability of the system.

- Better integration with the grid: predictive control can help ensure a stable and consistent power output from the wave energy conversion system, making it easier to integrate with the grid. This can help reduce the cost of energy storage and increase the overall efficiency of the system.

- Enhanced safety: predictive control can help ensure the safety of the system by monitoring and adjusting the motion of the point absorber to prevent excessive loading or motion. This can help prevent accidents and reduce the risk of damage to the system or surrounding infrastructure (Min Lin *et al.* 2011).

Overall, integrating predictive control into a wave energy conversion system based on a point absorber can help improve energy capture, reduce stress on components, increase reliability, improve grid integration, and enhance safety.

6.1 Model predictive control and procedure

Model Predictive Control (MPC) is a control technique that utilizes a mathematical model of the system being controlled to anticipate future behavior and optimize control actions for a specified time horizon. The fundamental principle of MPC is to solve an optimization problem at each control interval to determine the best control actions for the following time steps, given the current state of the system and any applicable constraints on the system inputs and outputs (Nguyen *et al.* 2019).

The design procedure for MPC typically includes the following steps:

- 1) System modeling: the first step involves creating a mathematical model of the system being controlled that captures the dynamic behavior of the system and the relationship between inputs and outputs.

- 2) Objective function formulation: the objective function is a mathematical expression that outlines the performance criteria that the controller should optimize, such as minimizing deviation from a desired setpoint, maximizing energy efficiency, or reducing operating costs.

- 3) Constraint definition: MPC considers constraints on system inputs and outputs, such as input variable limits, safety limits, or output variable constraints.

- 4) Prediction horizon selection: the prediction horizon determines the time length over which the model is utilized to anticipate the future behavior of the system. It should be long enough to capture system dynamics, but short enough to enable rapid response to changes.

- 5) Optimization problem solving: At each control interval, the controller solves an optimization problem to determine the optimal control actions over the prediction horizon that minimize the objective function, subject to the constraints.

6) Control actions implementation: the control actions derived from the optimization problem are implemented, and the process is repeated at the next control interval.

MPC is widely used in numerous industries, including chemical, process, and power plants, as well as robotics and autonomous vehicles. It offers a flexible and robust control strategy that can handle complex systems with nonlinearities and constraints.

6.2 Step of predictive control

a) Measurements of state variables

Acquire the necessary feedback signals based on the needs of the predictive model or for the purpose of generating references.

b) Generation of reference quantities

Produce the reference control variable $x(k)$ based on the particular use case.

c) Extrapolation

Predict the value of the reference control variable for the next instant $(k+1)$.

d) Creating models that operate in continuous time

If the continuous-time model of the power converter is a first-order system, it can be expressed as

$$\frac{dx}{dt} = Ax + Bu \quad (27)$$

Here, A and B refer to the converter parameters such as filter inductance, load resistance, dc-link capacitance, and so on. The variable to be controlled (voltage, current, power, torque, flux, etc.) is represented by x , and u represents the input variable (dc-voltage, grid voltage, etc.).

e) Creating models that operate in discrete time

To implement this strategy on digital control platforms, it is necessary to convert the continuous-time models to discrete time. In control theory, there are various discretization methods available, such as forward difference, backward difference, bilinear transformations (which are a combination of forward and backward difference), impulse-invariant and zero-order hold (Yaramasu and Wu 2017). Since the state equations describing the model in (27) are of first-order nature, an approximation of the derivative can be obtained using the forward or backward Euler method. Specifically, the forward Euler method considers the future sample $(k+1)$ and the present sample (k) , as described below

$$\frac{dx}{dt} = \frac{x(k+1) - x(k)}{T_s} \quad (28)$$

T_s : denotes the sampling interval used for discretization.

The discrete-time model for the control variable can be derived by inserting Eq. (28) into Eq. (27)

$$\frac{x(k+1) - x(k)}{T_s} = Ax(k) + Bu(k) \quad (29)$$

$$x(k+1) = (1 + AT_s)x(k) + BT_s u(k) \quad (30)$$

The backward Euler method offers an estimation of the derivative by utilizing both the present (k) and past $(k-1)$ samples.

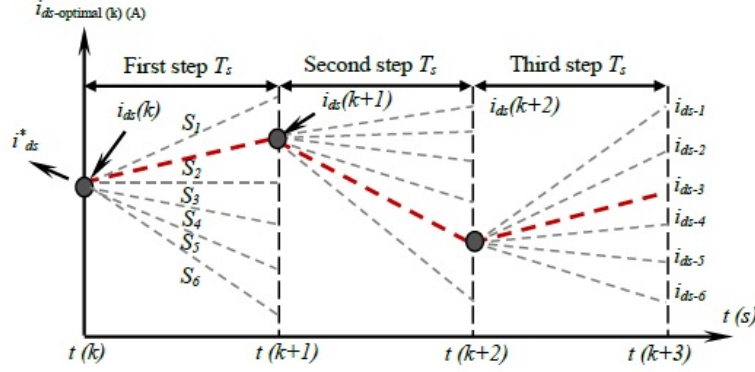


Fig. 11 Two-step prediction horizon in model predictive strategy

$$\frac{dx}{dt} = \frac{x(k) - x(k-1)}{T_s} \quad (31)$$

By utilizing the derivative estimation provided in Eq. (31), it is possible to discretize the continuous-time system expressed in Eq. (27) as follows

$$\frac{x(k) - x(k-1)}{T_s} = Ax(k) + Bu(k) \quad (32)$$

$$x(k) = \frac{1}{(1-AT_s)}x(k-1) + \frac{BT_s}{(1-AT_s)}u(k) \quad (33)$$

By moving the aforementioned variables to the next sample point in the future

$$x(k+1) = \frac{1}{(1-AT_s)}x(k) + \frac{BT_s}{(1-AT_s)}u(k+1) \quad (34)$$

In this equation, $u(k+1)$ refers to the predicted input.

f) Prediction

With the help of discrete-time models, the future behavior of control variables can be predicted using present sampling instant (k) measurements and past sample optimal variable $x(k)$.

g) Minimizing the cost function

Finally, a cost function g_k is utilized to compare the predicted variables $x_1(k+1)$, $x_2(k+1)$, $x_3(k+1)$, $x_4(k+1)$, and $x_5(k+1)$ with their corresponding reference value $x_{ref}(k+1)$.

$$g(k) = |x_p(k+1) - x_{ref}(k+1)|^2 \quad (35)$$

The objective of optimizing the cost function is to achieve a value of g that is as close to zero as possible. The switching state that minimizes the cost function is then selected and applied at the next sampling instant (Ataei *et al.* 2015).

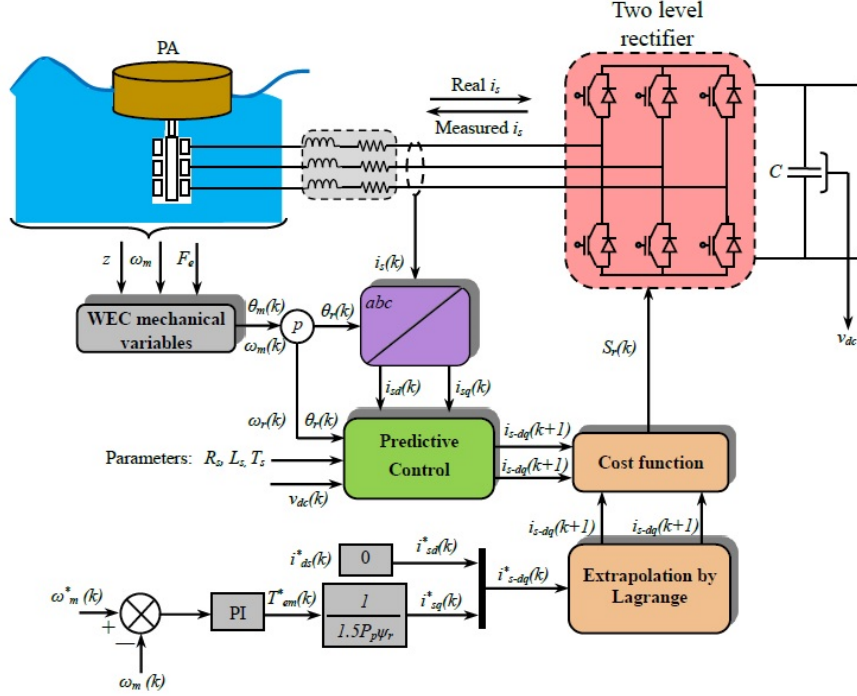


Fig. 12 Process diagram for the PCC algorithm on the LPMSG-side 2L-VSR

6.3 Predictive control scheme for the generator side converter

The block diagram depicted in Fig. 12 illustrates the predictive current control approach for an LPMSG equipped with 2L-VSR. By making minor adjustments to the block diagram, especially in the reference current computation, the predictive current control method can also be applied to another system based wave energy. The objective of the control scheme implemented on the generator side is to execute maximum power point tracking, where the generator currents are regulated in the dq frame. The design of the control approach is comprised of five key steps, which are elucidated below (Yamasu *et al.* 2016).

The predictive current control design is formulated based on the feedback signals, which comprise of various parameters such as the DC-link capacitor voltage $v_{dc}(k)$, three-phase generator/converter currents $i_s(k)$, and the mechanical speed $\omega_m(k)$ and position $\theta_m(k)$ of the generator rotor. To implement the predictive current control approach, the generator currents are measured in reverse direction (from VSR to LPMSG) to enable adoption of the motor model. Additionally, the PTO power and the wave speed $v_w(k)$ data are necessary to determine the reference currents. By multiplying the generator pole pairs with $\omega_m(k)$ and $\theta_m(k)$, the equivalent electrical speed $\omega_r(k)$ and position $\theta_r(k)$ can be computed. The electrical rotor position $\omega_r(k)$ is subsequently utilized to convert the three-phase currents into the dq-frame.

To compute the forecasted current at the t_{k+1} moment, it is possible to use Euler's formula to estimate the discrete current prediction equations of the dq axes, by disregarding the stator interaction. The approximation can be expressed as follows

$$\left\{ \begin{array}{l} i_d(k+1) = \left(1 - \frac{R_s T_s}{L_d}\right) i_d(k) - \left(\frac{\omega_r(k) L_d T_s}{L_q}\right) i_q(k) \\ \quad + \left(\frac{T_s}{L_d}\right) v_d(k) \\ i_d(k+1) = \left(1 - \frac{R_s T_s}{L_q}\right) i_q(k) + \left(\frac{\omega_r(k) L_q T_s}{L_d}\right) i_d(k) \\ \quad + \left(\frac{T_s}{L_q}\right) v_q(k) - \left(\frac{\omega_r(k) \psi_{PM} T_s}{L_q}\right) \end{array} \right. \quad (36)$$

where:

$i_d(k)$, $i_q(k)$, $v_d(k)$ and $v_q(k)$ are the dq components of output current and voltage at t_k instant.

$i_d(k+1)$ and $i_q(k+1)$ are the dq components of the predictive current value at t_{k+1} instant.

Eq. (36) is used to calculate the predicted current values $i_d(k+1)$ and $i_q(k+1)$. The reference current signal is generated by PI control using the reference voltage v_{dc}^* and DC-link voltage v_{dc} . In cases where the rectifier operates at unity power factor, the reactive current component i_d^* is zero, and the reference current corresponds to the active current component i_q^* (Venkata 2014).

The model of Eq. (36) can be written in the following matrix form

$$\begin{bmatrix} i_{ds}(k+1) \\ i_{qs}(k+1) \end{bmatrix} = \begin{bmatrix} 1 - \frac{R_s T_s}{L_s} & \omega_r(k) T_s \\ -\omega_r(k) T_s & 1 - \frac{R_s T_s}{L_s} \end{bmatrix} \begin{bmatrix} i_{ds}(k) \\ i_{qs}(k) \end{bmatrix} \\ + \begin{bmatrix} \frac{T_s}{L_s} & 0 \\ 0 & \frac{T_s}{L_s} \end{bmatrix} \begin{bmatrix} v_{ds}(k) \\ v_{qs}(k) \end{bmatrix} + \begin{bmatrix} 0 \\ -\frac{\omega_r(k) \psi_{PM} T_s}{L_s} \end{bmatrix} \quad (37)$$

where

$$\begin{bmatrix} v_{ds}(k) \\ v_{qs}(k) \end{bmatrix} = \begin{bmatrix} v_{dc}(k) \\ v_{dc}(k) \end{bmatrix} \begin{bmatrix} S_{dr1}(k) \\ S_{qr1}(k) \end{bmatrix}$$

Generating Feedback Signals

The measurement of the DC-link involves capturing the voltage across two capacitors. The DC-branch currents are estimated by utilizing the grid-side currents and optimal switching states of the NPC inverter. All other measurements are identical to those employed in the control system for the BTB 2L-VSC.

Calculating and extrapolating current reference values

To determine the LPMSG current error at the $(k+1)$ sampling instance, the reference currents are extrapolated to the $(k+1)$ state. Since i_{ds}^* is consistently zero in ZDC control, there is no requirement for extrapolation. In the steady state, extrapolation is unnecessary for i_{qs}^* . To enhance the transient performance, a first-order Lagrange extrapolation is executed utilizing the following general form:

$$\begin{cases} i_{sd}^*(k+1) = 2i_{sd}^*(k) - i_{sd}^*(k-1) \\ i_{sq}^*(k+1) = 2i_{sq}^*(k) - i_{sq}^*(k-1) \end{cases} \quad (38)$$

Predicting future LPMSG current behavior

The voltages at the NPC rectifier terminal are estimated by using the measured DC-link capacitor voltage and the switching signals in the dq-frame (Pinheiro Da Silva *et al.* 2022).

$$\begin{bmatrix} v_{ds}(k) \\ v_{qs}(k) \end{bmatrix} = v_{dc}(k) \begin{bmatrix} S_{dr1}(k) \\ S_{qr1}(k) \end{bmatrix} \quad (39)$$

The switching signals in the dq-frame are associated with the signals in the natural frame.

One can derive the dq-axis switching signals by calculating them from the intrinsic switching signals.

$$\begin{bmatrix} S_{drj}(k) \\ S_{qrj}(k) \end{bmatrix} = \begin{bmatrix} T_{\alpha\beta/dq} \end{bmatrix} \frac{2}{3} \begin{bmatrix} T_{abc/\alpha\beta} \end{bmatrix} \begin{bmatrix} S_{arj}(k) \\ S_{brj}(k) \\ S_{crj}(k) \end{bmatrix}, j \in \{1, 2\} \quad (40)$$

where

$$\begin{bmatrix} T_{\alpha\beta/dq} \end{bmatrix} = \begin{bmatrix} \cos \theta_r(k) & \sin \theta_r(k) \\ -\sin \theta_r(k) & \cos \theta_r(k) \end{bmatrix}$$

$$\begin{bmatrix} T_{abc/\alpha\beta} \end{bmatrix} = \begin{bmatrix} 1 & -\frac{1}{2} & -\frac{1}{2} \\ 0 & \frac{\sqrt{3}}{2} & -\frac{\sqrt{3}}{2} \end{bmatrix}$$

Finally, we can formulate the overall sampled-data model to predict future dq-axis current values by combining Eqs. (37) and (39). This formulation is expressed in terms of the 2L-VSR switching signals.

$$\begin{aligned} \begin{bmatrix} i_{ds}(k+1) \\ i_{qs}(k+1) \end{bmatrix} &= \begin{bmatrix} 1 - \frac{R_s T_s}{L_s} & \omega_r(k) T_s \\ -\omega_r(k) T_s & 1 - \frac{R_s T_s}{L_s} \end{bmatrix} \begin{bmatrix} i_{ds}(k) \\ i_{qs}(k) \end{bmatrix} \\ &+ \begin{bmatrix} \frac{T_s}{L_s} & 0 \\ 0 & \frac{T_s}{L_s} \end{bmatrix} \left(v_{dc}(k) \begin{bmatrix} S_{dr1}(k) \\ S_{qr1}(k) \end{bmatrix} \right) \\ &+ \begin{bmatrix} 0 \\ -\frac{\omega_r(k) \psi_{PM} T_s}{L_s} \end{bmatrix} \end{aligned} \quad (41)$$

There are eight different combinations for the switching signals, which are illustrated below

$$\begin{aligned} S_r(k) &\in [S_{ar}(k), S_{br}(k), S_{cr}(k)] \\ &\in [0, 0, 0], [1, 0, 0], [1, 1, 0], \\ &[0, 1, 0], [0, 1, 1], [0, 0, 1], [1, 0, 1], [1, 1, 1] \end{aligned} \quad (42)$$

Fig. 11 shows the operating principle for predicting current two step prediction horizon, assuming that the converter has 6 switching states (Singh *et al.* 2021). These 6 possible switching states lead to 6 predictions for the variable to be controlled. In contrast to classical control techniques that only observe past and present values of the variable, the proposed MPC approach takes into account the past, present, and future of the variable.

Minimizing the cost function is the main objective of the predictive current control technique, which focuses on controlling the dq-axis LPMSG currents. These currents can be expressed as two separate sub-cost functions, as outlined below

$$\begin{cases} g_{id}(k) = \left(\hat{i}_{ds}^*(k+1) - i_{ds-p}(k+1) \right)^2 \\ g_{iq}(k) = \left(\hat{i}_{qs}^*(k+1) - i_{qs-p}(k+1) \right)^2 \end{cases} \quad (43)$$

As shown below, the overall cost function on the generator side combines the previously mentioned sub-cost functions using the following weight factors

$$g(k) = \lambda_{id} g_{id}(k) + \lambda_{iq} g_{iq}(k) \quad (44)$$

where:

The variables λ_{id} and λ_{iq} represent the weighting factors.

6.4 Proposed predictive control model for grid side converter

The depicted model predictive control scheme in Fig. 13 is straightforward and easy to comprehend. The implementation process is outlined as follows

• Measure of :

Grid voltages: $v_{ag}(k)$ and $v_{bg}(k)$, ($v_{cg}(k) = -v_{ag}(k) - v_{bg}(k)$).

Grid currents: $i_{ag}(k)$ and $i_{bg}(k)$, ($i_{cg}(k) = -i_{ag}(k) - i_{bg}(k)$).

DC-link capacitor voltage $v_{dc}(k)$.

A total of three voltage sensors and two current sensors are necessary for a three-phase balanced system with symmetrical grid voltages.

• The grid voltage angle, $\theta_g(k)$, can be obtained using a synchronous reference frame phase-locked loop (PLL) [56].

• The grid voltages and currents, v and i , respectively, can be converted from the natural (abc) frame to the synchronous (dq) frame, resulting in $v_{dg}(k)$, $v_{qg}(k)$, $i_{dg}(k)$, and $i_{qg}(k)$.

The grid currents in a natural frame (abc) can be represented as a function of the inverter voltages, grid voltages, and filter inductance.

$$\frac{di_g}{dt} = \frac{1}{L_g} \left(-R_g i_g - v_g + v_i \right) \quad (45)$$

For easier design and control, the natural frame grid voltages and currents are converted to the synchronous frame. By converting the natural frame currents to the synchronous frame (dq), they can be expressed in state-space form as follows (Ahsan Said *et al.* 2022)

$$\begin{aligned} \begin{bmatrix} \frac{di_{dg}}{dt} \\ \frac{di_{qg}}{dt} \end{bmatrix} &= \begin{bmatrix} -\frac{R_g}{L_g} & \omega_g \\ -\omega_g & -\frac{R_g}{L_g} \end{bmatrix} \begin{bmatrix} i_{dg} \\ i_{qg} \end{bmatrix} \\ &+ \begin{bmatrix} \frac{T_s}{L_g} & 0 \\ 0 & \frac{T_s}{L_g} \end{bmatrix} \begin{bmatrix} v_{di} \\ v_{qi} \end{bmatrix} + \begin{bmatrix} -\frac{1}{L_g} & 0 \\ 0 & -\frac{1}{L_g} \end{bmatrix} \begin{bmatrix} v_{dg} \\ v_{qg} \end{bmatrix} \end{aligned} \quad (46)$$

The estimated inverter voltages for the d- and q-axis are represented by v_{di} and v_{qi} , respectively. These values are obtained by applying abc/dq transformation to the natural frame inverter voltages v_{an} , v_{bn} , and v_{cn} .

To obtain a one-step prediction for the d and q-axis grid currents, the discrete-time model can be derived from equation (46), as shown below

$$\begin{aligned} \begin{bmatrix} i_{dg}(k+1) \\ i_{qg}(k+1) \end{bmatrix} &= \begin{bmatrix} -\frac{R_g T_s}{L_g} & \omega_g(k) T_s \\ -\omega_g(k) T_s & -\frac{R_g T_s}{L_g} \end{bmatrix} \begin{bmatrix} i_{dg}(k) \\ i_{qg}(k) \end{bmatrix} \\ &+ \begin{bmatrix} \frac{T_s}{L_g} & 0 \\ 0 & \frac{T_s}{L_g} \end{bmatrix} \begin{bmatrix} v_{di}(k) \\ v_{qi}(k) \end{bmatrix} + \begin{bmatrix} -\frac{1}{L_g} & 0 \\ 0 & -\frac{1}{L_g} \end{bmatrix} \begin{bmatrix} v_{dg}(k) \\ v_{qg}(k) \end{bmatrix} \end{aligned} \quad (47)$$

• The q-axis reference current, $i_{qg}^*(k)$, can be obtained from $Q_g^*(k)$. Referring to Eq. (26) and use the grid voltage orientation, $i_{qg}^*(k)$ can be calculated as follows

$$i_{qg}^*(k) = -\frac{Q_g^*(k)}{1.5v_{dg}(k)} \quad (48)$$

•- The d-axis reference current, $i_{dg}^*(k)$, can be obtained to represent the active power of the system. Neglecting losses in the inverter, the active power on the AC side P_g , is equal to the DC power and can be expressed as follows (Ronald Repi and Tirta Diputra 2022):

$$P_g = \frac{3}{2} v_{dg} i_{dg} = v_{dc} i_{dc} \quad (49)$$

The PI controller maintains the net DC-bus voltage v_{dc} , at its reference value v_{dc}^* , during steady-state. The $i_{dg}^*(k)$ is generated by this PI controller based on the current operating conditions.

•- To extrapolate reference currents from the k -th state to the $(k+1)$ state, we adopt the fourth-order Lagrange extrapolation method in our research (Binh *et al.* 2016).

$$\begin{cases} i_{dg}^*(k+1) = 4i_{dg}^*(k) - 6i_{dg}^*(k-1) + 4i_{dg}^*(k-2) - i_{dg}^*(k-3) \\ i_{qg}^*(k+1) = 4i_{qg}^*(k) - 6i_{qg}^*(k-1) + 4i_{qg}^*(k-2) - i_{qg}^*(k-3) \end{cases} \quad (50)$$

The relationship between the currents and voltages of the dc-link capacitor can be expressed in continuous time as follows

$$\frac{dv_{dc}}{dt} = \frac{1}{C} i_{dc} \quad (51)$$

By utilizing the dc link voltage model presented in Eq. (51), we can derive a discrete-time model for the dc-link capacitor voltages when $j = 1$, as follows

$$v_{dc}(k+1) = v_{dc}(k) + \frac{T_s}{C} i_{dc}(k) \quad (52)$$

Here: T_s refers to the sampling time and C represents the capacitance of the dc-capacitors. The current flowing through the dc-capacitors is represented as i_{dc} (Ringwood *et al.* 2019). The dc-link capacitor currents can be expressed as a function of the three-phase grid currents and gain K_{lx} , as shown below

$$i_{dc}(k+1) = \sum_{x=a,b,c} K_{lx}(k+1) i_{xg}(k+1) \quad (53)$$

The gain K_{lx} depend on the switching states of the inverter, as illustrated below

$$K_{lx} = \text{sign}(0 - S_x) \quad (54)$$

The Signum function (sign) produces an output value of -1, 0, or +1.

7. Simulation results and analysis

In this section, we present the simulation outcomes of a point absorber WEC based on a 200 kW LPMSG technology. The LPMSG-based WEC system shown in Fig. 1 was modeled in the Matlab/Simulink environment. We also provide the LPMSG and the grid connection parameters in Tables 2 and 3 respectively. The effectiveness and practicality of employing predictive control on the side generator and grid via a back-to-back converter topology under stochastic wave speed fluctuations are examined.

The two inverters under consideration are assumed to be ideal, and the switching frequency of the grid-side inverter is set equal to that of the inverter controlling the LPMSG. The values of the filter resistance, filter inductance, capacitor capacity, and DC link voltage have been selected.

The simulation of the point absorber model with grid connection aims to accomplish three goals: firstly to examine the behavior of key system variables over time, secondly to verify the successful injection of power generated by the PTO into the grid, and thirdly to confirm that current is injected into

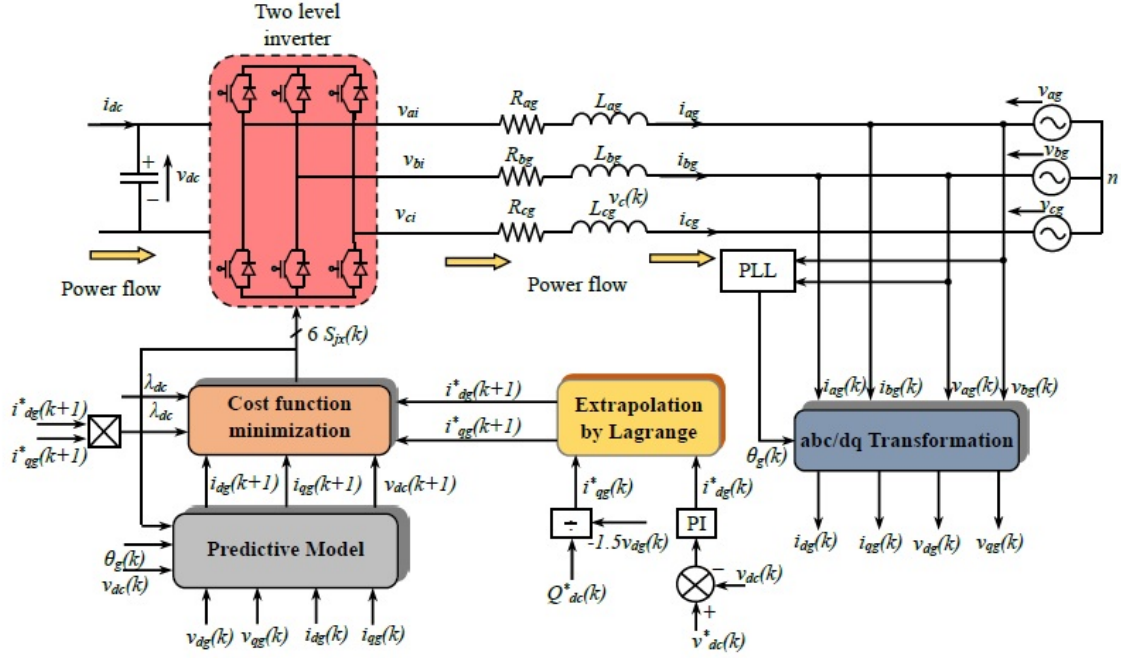


Fig. 13 Process diagram for the predictive control algorithm on the grid-side 2L-VSC

the grid with unity power factor. To achieve these objectives, a simulation time of 60 seconds was deemed sufficient. Fig. 14 displays the trends over time of several variables, including the applied wave form, the rod speed, the buoy position and the point absorber reaction.

To assess the transient and steady state performances of the studied predictive controllers under abrupt changes in wave speed, simulation responses were generated and presented in Fig. 15. Fig. 15(a) illustrates the LPMSG rotational velocity response to wave speed under the predictive model controllers, indicating favorable steady-state performance for both regulators.

The electromagnetic torque developed by the generator is display on Fig. 15(b).

As a result, it can be concluded that the DC voltage control shown in Fig. 22 is operating correctly and that the power generated by the PTO is injected directly into the grid, since the DC link voltage of the capacitor remains almost constant. A constant DC link voltage implies a steady energy storage in the capacitor over time.

The distortion in the Figs. 16 and 18 of the stator voltage and current waveforms of the LPMSG is caused by the diode's natural commutation.

Although shown in Figs. 17, 19 and 20 which show the zoom, the fundamental components of stator voltage and current are in phase, indicating the achievement of unity power factor operation. The LPMSG's three-phase currents generate harmonics, which result in ripples in the electromagnetic torque (T_{em}). The control strategy ensures that the dc-link current i_{dc} is maintained at its reference value, while the grid-side inverter regulates the net dc-bus voltage and reactive power to their respective reference values (Fig. 21).

Figs. 23 and 25 demonstrate the grid voltage and current respectively, and their magnified views on Figs. 24 and 26. These provide verification of the unity power factor of the OWC. These results

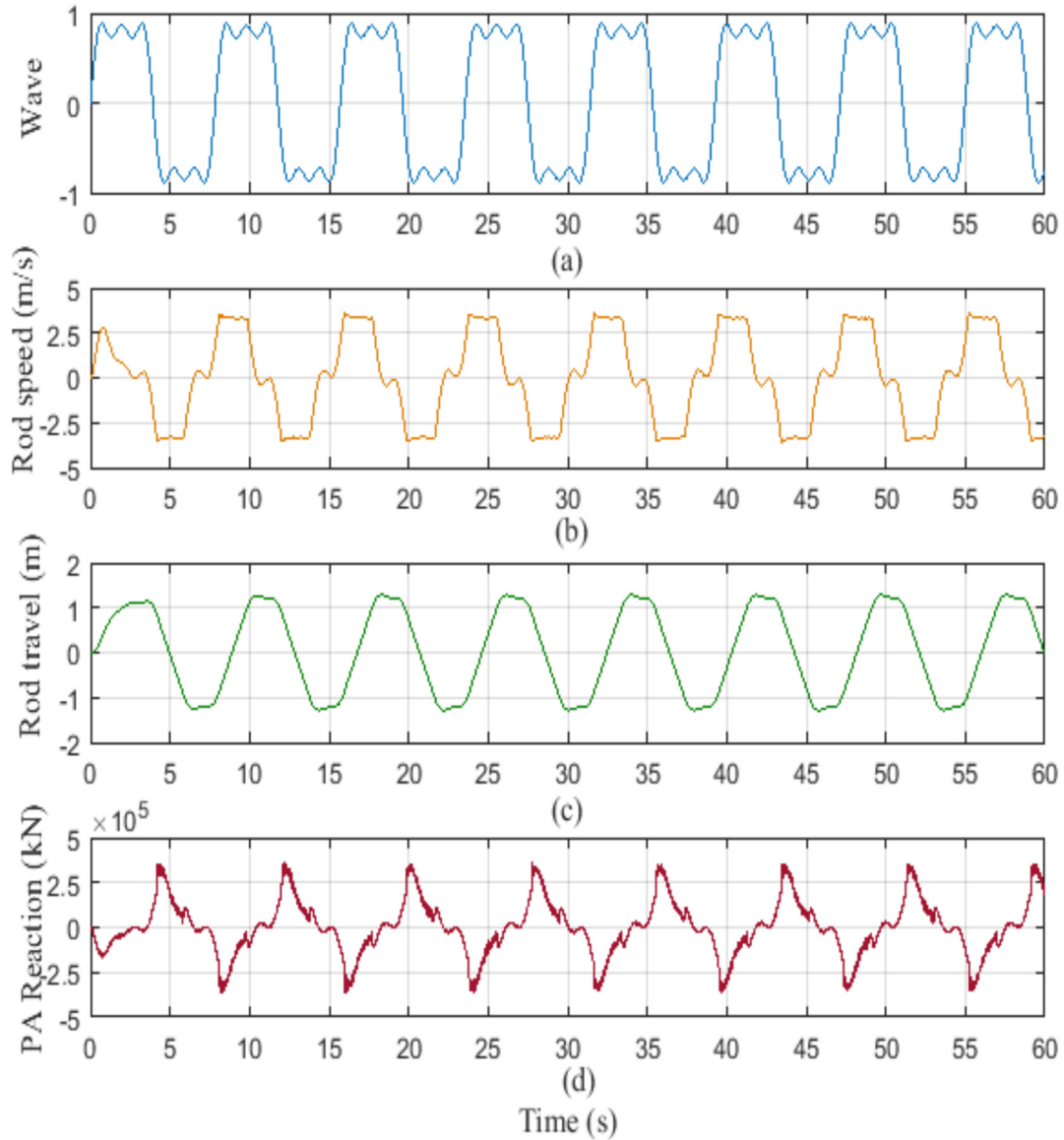


Fig. 14 Time evolution of key variables in the WEC based point absorber model

establish that the BTB inverter is efficiently controlled, as validated by the constant maintenance of the DC bus voltage.

One can observe that the fluctuations in the DC link voltage and grid current waveform are correlated with the oscillations in the speed of the generator.

The grid current components along the q and q axis are illustrated in Fig. 27, there is a good decoupling of the two components according to the control law applied. From Fig. 28, the proposed predictive controller exhibits exceptional transient response during the linear change of Q_g^* value from 10 VAR to 15 VAR while regulating the net DC-bus voltage and reactive power at their

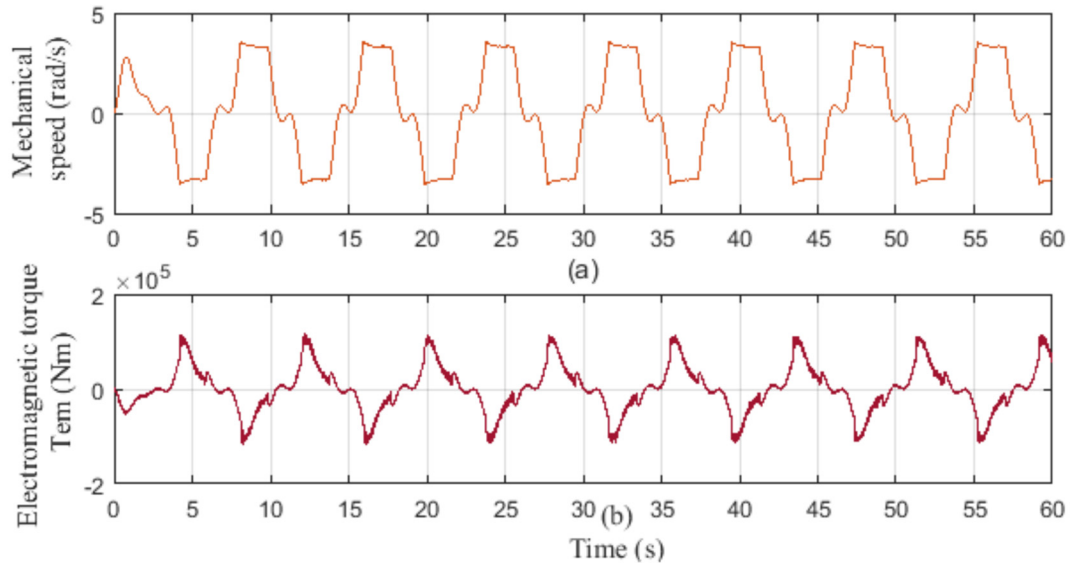


Fig. 15 Mechanical variables of the LPSMG: (a) speed of the generator and (b) electromagnetic torque developed by the generator

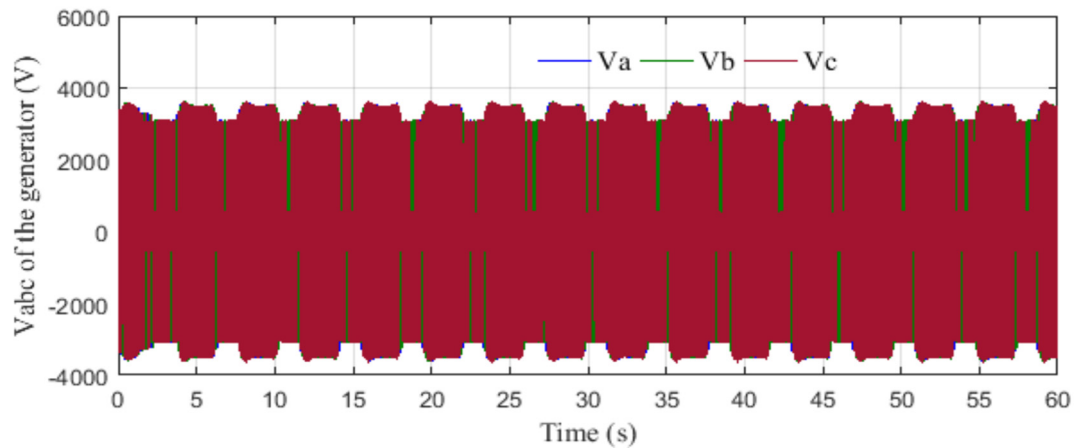


Fig. 16 Three-phase LPMSG phase voltages waveforms under rated operating condition with BTB converter

reference values. Once the LPMSG speed reaches the new reference value, the input power and the grid power values stabilize at a new steady-state value. Although the net DC-bus voltage deviates from its reference value during this period, the rectifier converter's control strategy effectively balances the DC-link capacitor voltages.

The Fig. 29 with the zoom on Fig. 30 shows a grid current of 600 A and a zero phase angle between the grid voltage and current due to the zero reactive power reference. The active and reactive power apparent power are recorded as 300 kW and 10 VAR, respectively.

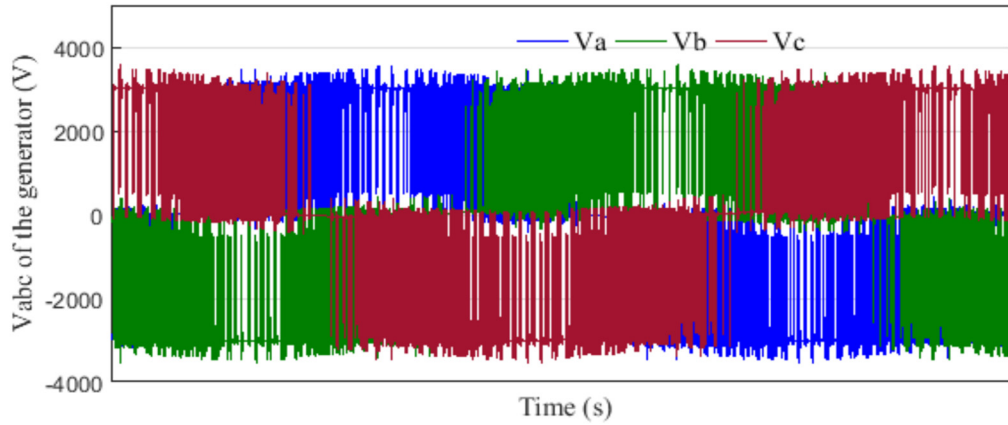


Fig. 17 Zoom of the three phase voltages of the generator

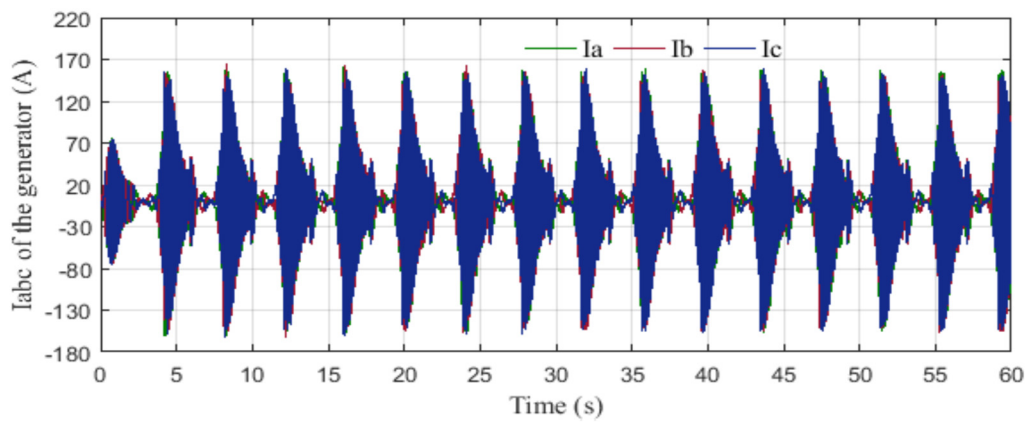


Fig. 18 Three-phase LPMSG phase currents waveforms under rated operating condition with BTB converter

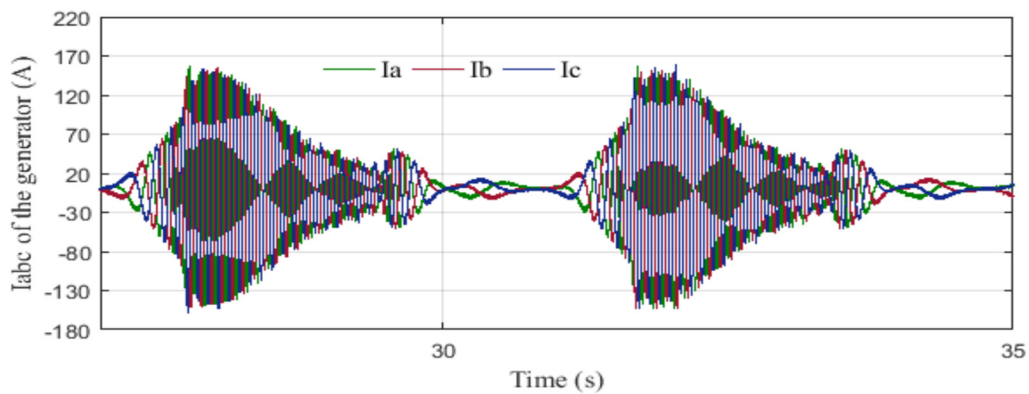


Fig. 19 Zoom of three-phase LPMSG phase currents waveforms under rated operating condition with BTB converter

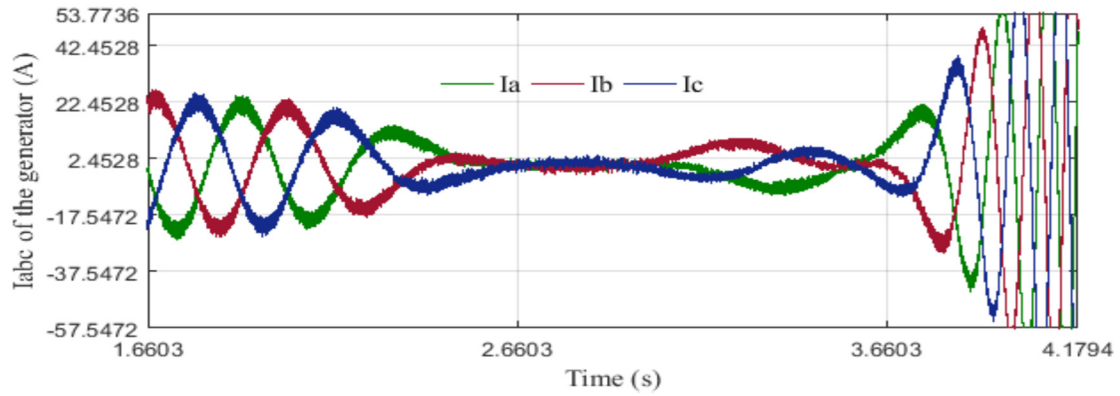


Fig. 20 Zoom of three-phase LPMSG phase currents between $t=1.66$ s and $t=4.17$ s

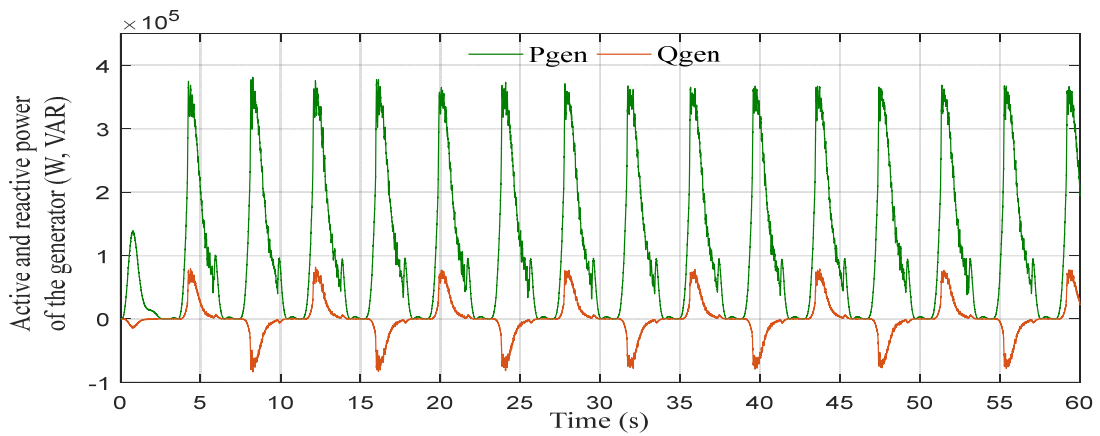


Fig. 21 Performance tracking of active and reactive power delivered by the generator

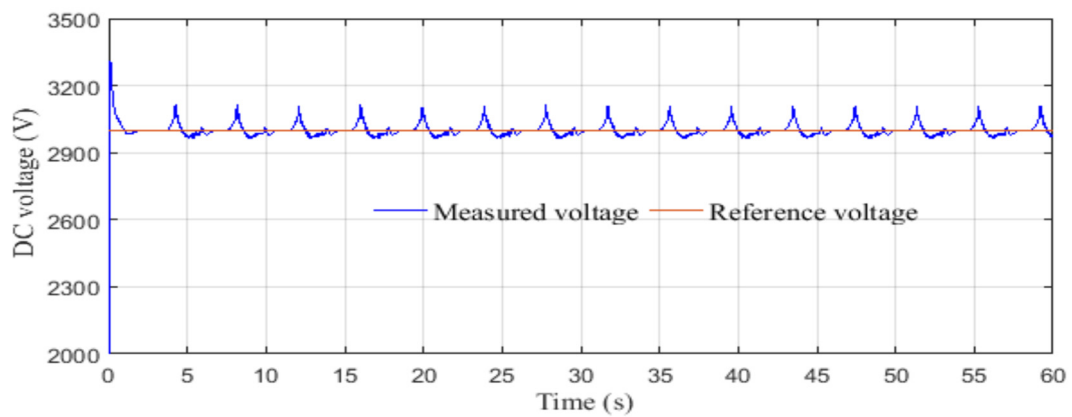


Fig. 22 DC bus voltage under wave fluctuation

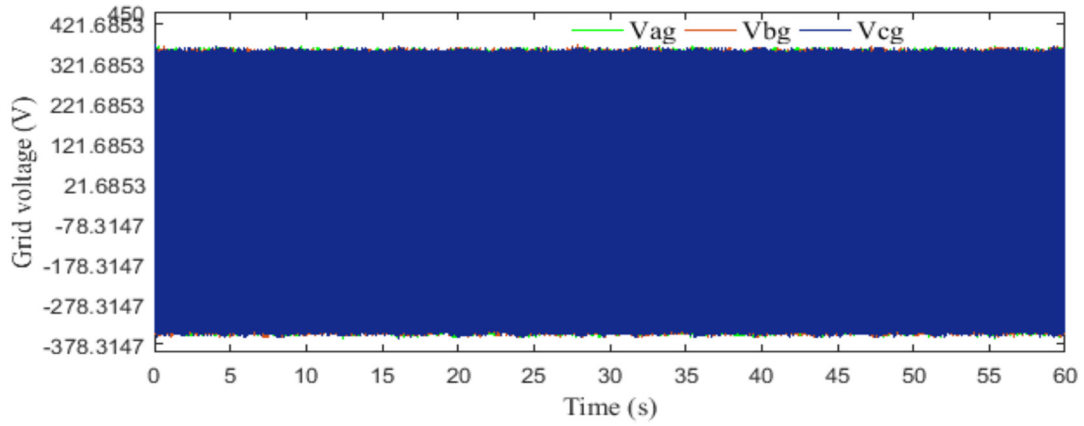


Fig. 23 Three phase grid voltages

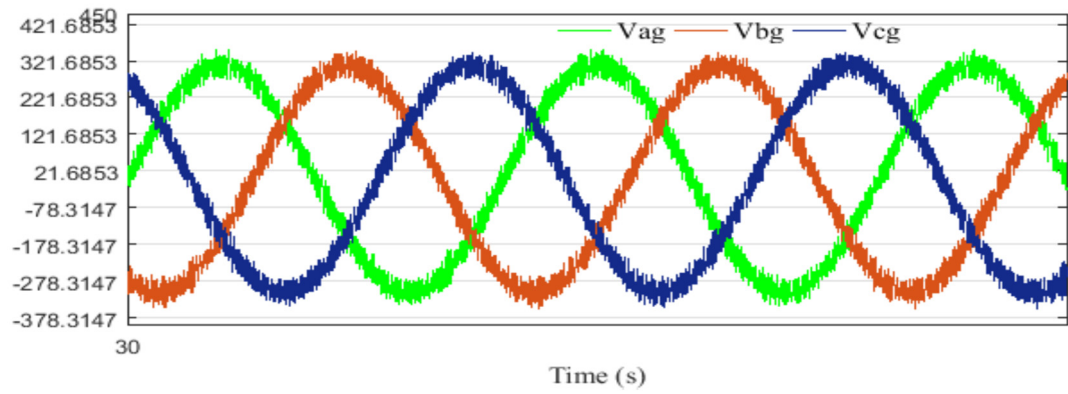


Fig. 24 Zoom of three phase grid voltages

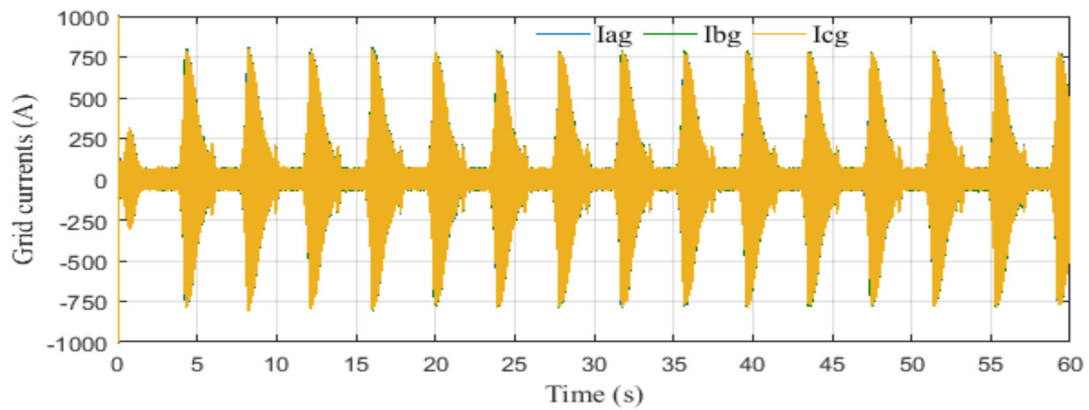


Fig. 25 Three phase grid currents

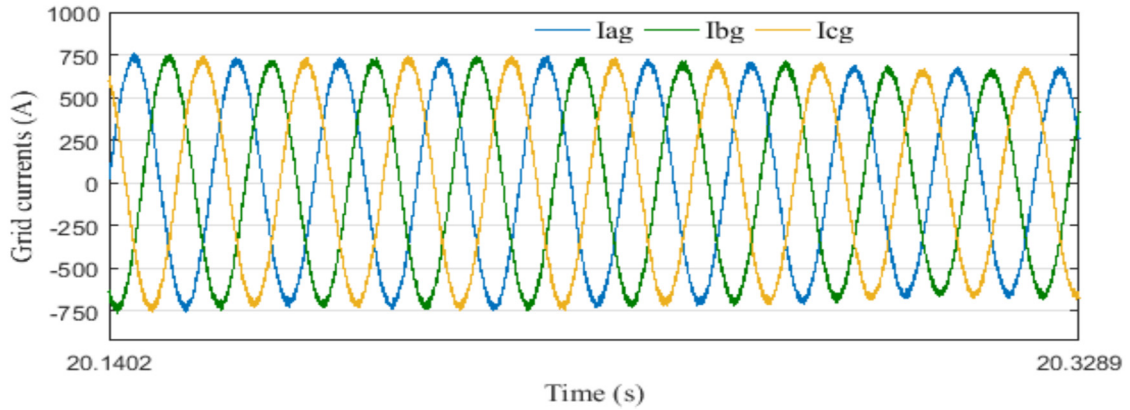


Fig. 26 Zoom of three phase grid current

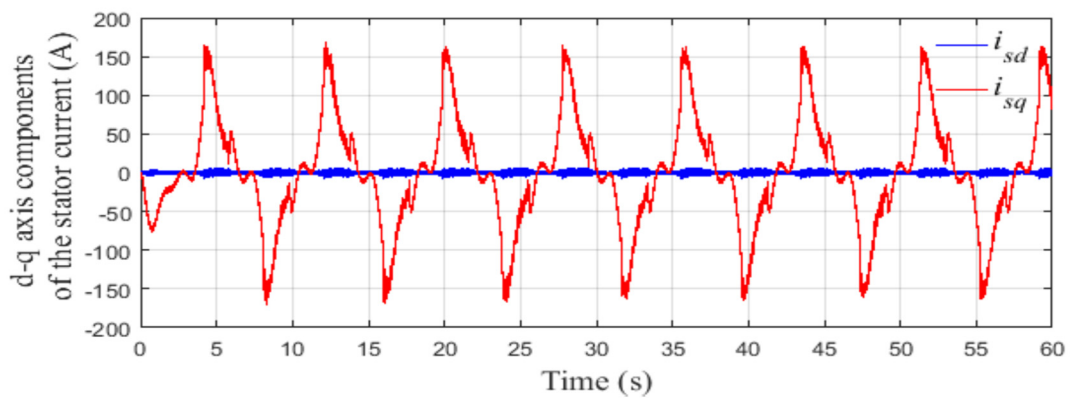


Fig. 27 The components of the grid current along the d and q axis

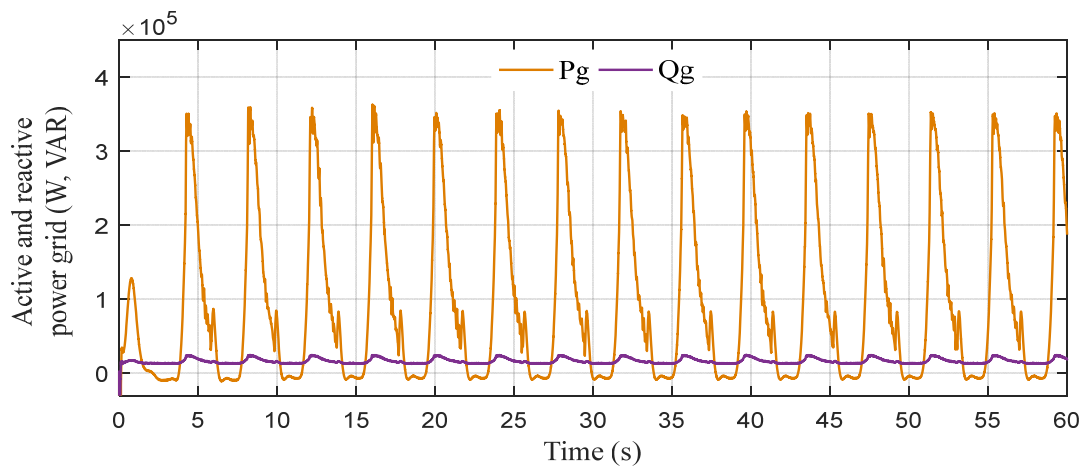


Fig. 28 Performance tracking of active and reactive power grid

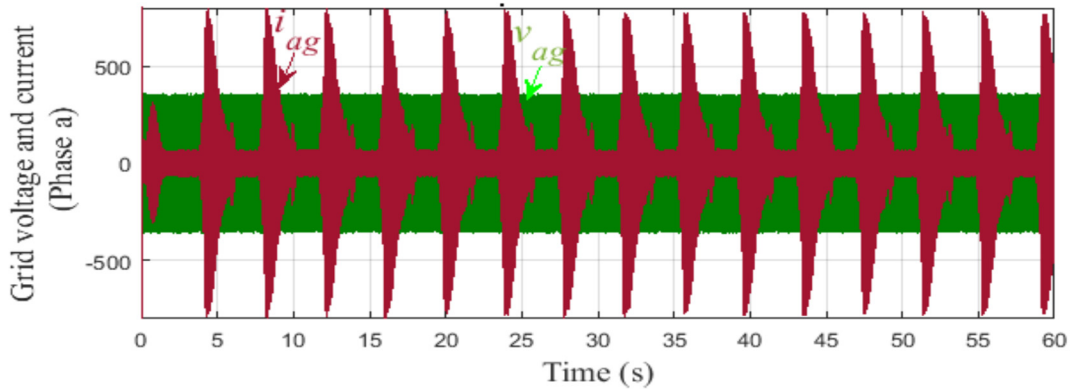


Fig. 29 Time evolution of phase (a) of grid voltage and current

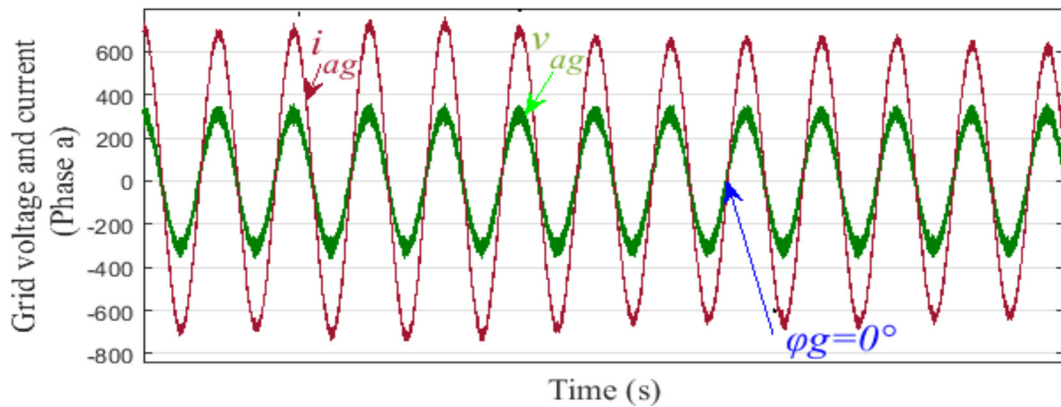


Fig. 30 Zoom and detailed view of phase (a) of grid voltage and current

Figs. 29 and 30 shows a detailed plot of the voltage and current of phase a at the grid section and their zoom, to verify the power factor. The voltage waveform is represented by the red line, while the current waveform is represented by the green line. It is evident that both waveforms are sinusoidal and in phase, indicating successful injection of current into the grid with unity power factor, as intended. It is worth mentioning that the generator's rated output is less than the mechanical input power during this operation. While operating, it was observed that the rectifier converter and the NPC inverters had switching frequencies of 2000 Hz and 1900 Hz, respectively.

The analysis of the simulation results carried out makes it possible to highlight any shortcomings or obstacles to the predictive control system, as well as opportunities for improvement. The results reveal good stability of the studied system and very limited noise and vibration levels, which may indicate the effectiveness of the control approach and the proposed system design. The obtained simulation results and elaborate discussions play a central role in evaluating the effectiveness and possibilities of predictive control for PA-LPMSG systems and can guide further research and progress in this area.

8. Conclusions

This article has presented a comprehensive study on the modeling and control of a point absorber wave energy converter that is connected to the electric grid using a PMSG-based power converter. The research work has successfully demonstrated the potential of wave energy as a reliable and sustainable source of renewable energy. The control system developed in this study has shown promising results in ensuring optimal energy output and stable grid connection. However, there is still a significant amount of research required to improve the performance of wave energy converters and their integration into the electric grid.

Future research could focus on exploring new control strategies, improving the efficiency of the system, and reducing the overall cost of the technology. Additionally, research can be directed towards developing new materials and technologies to enhance the durability and reliability of wave energy converters in harsh marine environments. The findings of this study can have a significant impact on the development of wave energy technology and its integration into the electric grid, thus contributing to the overall goal of reducing greenhouse gas emissions and mitigating the effects of climate change.

In summary, the research presented in this article represents a significant step towards the commercialization of wave energy technology. The potential of wave energy to provide a sustainable and reliable source of energy cannot be overstated. It is crucial that research in this field continues to advance to fully realize the potential of this technology to address the challenges of climate change and meet the energy demands of the future.

Acknowledgments

The authors extend their appreciation to the deputyship for Research & Innovation, Ministry of Education in Saudi Arabia for funding this research work through the project number ISP22-5.

References

- Abdelkhalik, O., Robinett, R., Zou, S. Bacelli, G., Coe, R., Bull, D. Wilson, D. and Korde, U. (2016), "On the control design of wave energy converters with wave prediction", *J. Ocean Eng. Mar. Energ.*, **2**, 473-483. <https://doi.org/10.1007/s40722-016-0048-4>.
- Adaryani, M.R., Taher, S.A. and Guerrero, J.M. (2020), "Model predictive control of direct-drive wave power generation system connected to DC microgrid through DC cable", *Int. T. Elec. Energ. Syst.*, **30**(9), 12484. <https://doi.org/10.1002/2050-7038.12484>.
- Adaryani, M.R., Taher, S.A. and Guerrero, J.M. (2021), "Improved direct model predictive control for variable magnitude variable frequency wave energy converter connected to constant power load", *J. Energ. Storage*, **43**, <https://doi.org/10.1016/j.est.2021.103175>.
- Aguirre, A.S., Ulazia, A., Berastegui, G.I. and Saenz, J. (2021), "Extension and improvement of synchronous linear generator based point absorber operation in high wave excitation scenarios", *Ocean Eng.*, **239**, 109844. <https://doi.org/10.1016/j.oceaneng.2021.109844>.
- Ahsan Said, H., Violini, D.G. and Ringwood, J.V. (2022), "Wave-to-grid (W2G) control of a wave energy converter", *Energ. Convers. Management*, **14**, 100190. <https://doi.org/10.1016/j.ecmx.2022.100190>.
- Amon, E.A., Brekken, T.K.A. and Schacher, A.A. (2012), "Maximum power point tracking for ocean wave energy conversion", *IEEE T. Ind. Appl.*, **48**(3), 1079-1086, <https://doi.org/10.1109/TIA.2012.2190255>.

- Anderlini, E., Forehand, D.I.M., Bannon, E., Xiao, Q. and Abusara, M. (2018), "Reactive control of a two-body point absorber using reinforcement learning", *Ocean Eng.*, **148**, 650-658. <https://doi.org/10.1016/j.oceaneng.2017.08.017>.
- Artal-Sevil, J.S., Domínguez, J.A., El-Shalakany, H. and Dufo, R. (2018), "Modeling and simulation of a wave energy converter system. Case study: Point absorber", *Proceedings of the 13th International Conference on Ecological Vehicles and Renewable Energies (EVER)*, Monte Carlo, Monaco, 1-7. <https://doi.org/10.1109/EVER.2018.8362405>.
- Ataci, A., Rashidi, R., Nedaei, M. and Kurdestani, E. (2015), "Techno-economic viability of a hybrid wind and solar power system for electrification of a commercial building in Shiraz", *Adv. Energ. Res.*, **3**(4), 251-263. <http://dx.doi.org/10.12989/eri.2015.3.4.251>.
- Babes, B., Rahmani, L., Chaoui, A. and Hamouda, N. (2017), "Design and experimental validation of a digital predictive controller for variable-speed wind turbine systems", *J. Power Elec.*, **17**(1), 232-241. <https://doi.org/10.6113/JPE.2017.17.1.232>.
- Berkani, A., Negadi, K., Safa, A. and Marignetti, F. (2020), "Design and practical investigation of a model predictive control for power grid converter", *Tecnica Italiana-Italian J. Eng. Sci.*, **64**(2-4), 354-360. <https://doi.org/10.18280/ti-ijes.642-434>.
- Binh, P.C., Tri, N.M., Dung, D.T., Ahn, K.K., Kim, S.J. and Koo, W. (2016), "Analysis, design and experiment investigation of a novel wave energy converter", *IET Gener. Transm. Distrib.*, **10**, 460-469. <https://doi.org/10.1049/iet-gtd.2015.0821>.
- Casagrande, G. (2015), "Wave-to-wire model of a wave energy converter equipped with an all-electric power take-off", Master Thesis in Electrical Engineering.
- Da Silva, L.S.P., Ding, B., Guo, B. and Sergiienko, N.Y. (2022), "Wave energy converter modelling, control, and power take-off design", *In book: Modelling and Optimisation of Wave Energy Converters*. <https://doi.org/10.1201/9781003198956-3>.
- Duthoit, M. and Falzarano, J. (2018), "Assessment of the potential for the design of marine renewable energy systems", *Ocean Syst. Eng.*, **8**(2), 119-166. <https://doi.org/10.12989/ose.2018.8.2.119>.
- De Backer, G. (2009), "Hydrodynamic design optimization of wave energy converters consisting of heaving point absorbers", Ghent University. Faculty of Engineering, Ghent, Belgium.
- Eduard, M. and Yi-Hsiang, Y. (2015), "Review of marine hydrokinetic power generation and power plant", *Elec. Power Components Syst.*, **43**, <https://doi.org/10.1080/15325008.2015.1030519>.
- Eedara, A.K., Koritala, C.S. and Rayapudi, S.R. (2019), "Modified model predictive control of back-to-back T-type NPC converter interfacing wind turbine-driven PMSG and electric grid", *Arab. J. Sci. Eng.*, **44**, 7047-7065. <https://doi.org/10.1007/s13369-019-03775-0>.
- El-Shalakany, H., Jesús, A.S., Ballestín-Bernad, V., Navarro, D. and Antonio, J. (2022), "Ocean wave energy converters: Analysis, modeling, and simulation", *Some case studies. Renewable Energy and Power Quality J.*, **20**, 783-788. <https://doi.org/10.24084/repqj20.435>.
- Engin, C.D. and Yeşildirek, A. (2015), "Designing and modeling of a point absorber wave energy converter with hydraulic power take-off unit", *Proceedings of the 2015 4th International Conference on Electric Power and Energy Conversion Systems (EPECS)*, Sharjah, United Arab Emirates. <https://doi.org/10.1109/EPECS.2015.7368507>.
- Fabrizio, M., Haitao, Y. and Luigi, C. (2015), Special issue on "Marine Energy Conversion", *Adv. Mech. Eng.*, **7**(5), 1-2. <https://doi.org/10.1177/1687814015586529>.
- Faizal, M., Rafiuddin, A.M. and Young-Ho, L. (2014), "A design outline for floating point absorber wave energy converters", *Adv. Mech. Eng.*, 846097. <https://doi.org/10.1155/2014/846097>.
- Ghany, A.A., Shehata, E.G., Elsayed, A.H.M., Mohamed, Y.S., Haes Alhelou, H., Siano, P. and Diab, A.A.Z. (2021), "Novel switching frequency FCS-MPC of PMSG for grid-connected wind energy conversion system with coordinated low voltage ride through", *Electronics*, **10**(4), 492. <https://doi.org/10.3390/electronics10040492>.
- Giralda, P.R., Crespo, A.J.C., Coe, R.G., Tagliaferro, B., Domínguez, J.M., Bacelli, G. and Gesteira, M.G. (2021), "Modelling a heaving point-absorber with a closed-loop control system using the DualSPHysics code", *Energies*, **14**(3), 760. <https://doi.org/10.3390/en14030760>.

- Guo, B., Wang, T., Jin, S., Duan, S., Yang, K. and Zhao, Y.A. (2022), "Review of point absorber wave energy converters", *J. Mar. Sci. Eng.*, **10**, 1534. <https://doi.org/10.3390/jmse10101534>.
- Huang, X., Zhu, L., Wu, W., Lu, K., Wang, K. and Koh, C.S. (2021), "A global maximum power point tracking control strategy based on particle swarm optimization algorithm for point-absorber-type wave energy converters", *Proceedings of the IEEE 12th Energy Conversion Congress & Exposition - Asia (ECCE-Asia)*, Singapore. <https://doi.org/10.1109/ECCE-Asia49820.2021.9479115>.
- Hung, C.C. and Nguyen, T. (2022), "Adaptive backstepping control with grey theory for offshore platforms", *Ocean Syst. Eng.*, **12**(2), 159-172. <https://doi.org/10.12989/ose.2022.12.2.159>.
- Jingjin, X. and Lei, Z. (2013), "Dynamics and control of ocean wave energy converters", *Int. J. Dyn. Control*, **1**, 262-276. <https://doi.org/10.1007/s40435-013-0025-x>.
- Josset, C., Babarit, A. and Clément A.H. (2007), "Wave-to-wire model of the SEAREV wave energy converter", *Proceedings of the Institution of Mechanical Engineers, Part M: J. Engineering for the Maritime Environment*, **221**(2), 81-93. <https://doi.org/10.1243/14750902JEME48>.
- Lee, K., Jung, K., Suh, Y., Kim, C., Yoo, H. and Park, S. (2014), "Comparison of high power semiconductor devices losses in 5MW PMSG MV wind turbines", *Proceedings of the IEEE Applied Power Electronics Conference and Exposition - APEC 2014*, Fort Worth, TX, USA. <https://doi.org/10.1109/APEC.2014.6803657>.
- Lin, W.M., Hong, C.M., Ou, T.C. and Chiu, T.M. (2011), "Hybrid intelligent control of PMSG wind generation system using pitch angle control with RBFN", *J. Energ. Convers. Management*, **52**(2), 1244-1251. <https://doi.org/10.1016/j.enconman.2010.09.020>.
- Makhad, M., Zazi, M. and Loulijat, A. (2020), "Nonlinear control of WECS based on PMSG for optimal power extraction", *Int. J. Elec. Comput. Eng. (IJECE)*, **10**(3), 2815-2823. <http://doi.org/10.11591/ijece.v10i3.pp2815-2823>.
- Michael, L., Yu, Y.H., Kelley, R. and Carlos, M. (2014), "Development and demonstration of the WEC-sim wave energy converter simulation tool", *Marine Energy Technology Symposium*.
- Nguyen, C.U., Lee, S.Y., Huynh, T.C. and Kim, J.T. (2019), "Vibration characteristics of offshore wind turbine tower with gravity-based foundation under wave excitation", *Smart Struct. Syst.*, **23**(5), 405-420. <https://doi.org/10.12989/sss.2019.23.5.405>.
- Noman, M., Li, G., Wang, K. and Han, B. (2021), "Electrical control strategy for an ocean energy conversion system", *Prot. Control Mod. Power Syst.*, **6**(12). <https://doi.org/10.1186/s41601-021-00186-y>.
- Pastor, J. and Yucheng, L. (2014), "Time domain modeling and power output for a heaving point absorber wave energy converter", *Int. J. Energ. Environ. Eng.*, **5**(2-3), <https://doi.org/10.1007/s40095-014-0101-9>.
- Poguluri, S.K., Kim, D. and Bae, Y.H. (2022), "Performance assessment of pitch-type wave energy converter in irregular wave conditions on the basis of numerical investigation", *Ocean Syst. Eng.*, **12**(1), 23-38. <https://doi.org/10.12989/ose.2022.12.1.023>.
- Pranupa, S., Sriram, A.T. and Rao, S.N. (2022), "Wind energy conversion system using perturb & observe-based maximum power point approach interfaced with T-type three-level inverter connected to grid", *Clean Energy*, **6**(4), 534-549. <https://doi.org/10.1093/ce/zkac034>.
- Richter, M. (2011), Different model predictive control approaches for controlling point absorber wave energy converters.
- Richter, M., Magana, M., ESawodny, O. and Brekken, T.K.A. (2013), "Nonlinear model predictive control of a point absorber wave energy converter", *IEEE T. Sustain. Energ.*, **4**(1), 118-126. <https://doi.org/10.1109/TSSTE.2012.2202929>.
- Ringwood, J., Ferri, F., Tom, N., Ruehl, K., Faedo, N., Bacelli, G., Yu, Y. and Coe, RG. (2019), "The wave energy converter control competition: Overview", *Proceedings of the ASME 2019 38th International Conference on Ocean, Offshore and Arctic Engineering*, **10**, *Ocean Renewable Energy*. Glasgow, Scotland, UK. June 9-14. <https://doi.org/10.1115/OMAE2019-95216>.
- Ronald Repi, V.V. and Tirta Diputra, F. (2022), "Simulation and validation of floating-point absorber (FPA) wave energy converter (WEC) using open-source WEC-Sim simulation", *Proceedings of the AIP Conference*, 2664, 050003. <https://doi.org/10.1063/5.0108138>.

- Ruezga, A., Cañedo, J.M.C., Verduzco-Zapata, M.G. and Ocampo-Torres, F.J. (2021), "Performance analysis of a point-absorber wave energy converter with a single buoy composed of three rigidly coupled structures", *Int. J. Mar. Energ.*, **4**(2), 37-45. <https://doi.org/10.36688/imej.4.37-45>.
- Shengquan, L., Juan, L., Yongwei, T., Yanqiu, S. and Wei, C. (2020), "Model-based model predictive control for a direct-driven permanent magnet synchronous generator with internal and external disturbances", *Transactions of the Institute of Measurement and Control*, **42**(3), 586-597. <https://doi.org/10.1177/0142331219878574>.
- Singh, A. (2020), "Development and control of generator-converter topology for direct-drive wind turbines, rotating machinery", *Intech Open*. <https://doi.org/10.5772/intechopen.85877>.
- Singh, D., Singh, A., Ranjan Paul, A. and Samad, A. (2021), "Design and simulation of point absorber wave energy converter", *E3S Web of Conferences*, **321**, 03003. <https://doi.org/10.1051/e3sconf/202132103003>.
- Srivastava, A. and Bajpai, R.S. (2022), "Model predictive control of grid-connected wind energy conversion system", *IETE J. Res.*, **68**(5), 3474-3486. <https://doi.org/10.1080/03772063.2020.1768905>.
- Sunn, Y., Zhao, Y., Dou, Z., Li, Y. and Guo, L. (2020), "Model predictive virtual synchronous control of permanent magnet synchronous generator-based wind power system", *Energies*, **13**(19), 5022. <https://doi.org/10.3390/en13195022>.
- Tagliaferro, B., Martínez-Estévez, I., Domínguez, J.M., Crespo, A.J.C., Göteman, M., Engström, J. and Gómez-Gesteira, M. (2022), "A numerical study of a taut-moored point-absorber wave energy converter with a linear power take-off system under extreme wave conditions", *Appl. Energ.*, **311**, <https://doi.org/10.1016/j.apenergy.2022.118629>.
- Venkata, Y. (2014), "Predictive control of multilevel converters for megawatt wind energy conversion systems", <https://doi.org/10.13140/RG.2.1.3620.2400>.
- Wan, Z., Zheng, H., Sun, K., Zhang, D., Yao, Z. and Song, T. (2019), "Simulation of wave energy converter with designed pendulum-slope combination", *Energ. Procedia*, **158**, 733-737. <https://doi.org/10.1016/j.egypro.2019.01.196>.
- Wang, L., Isberg, J. and Tedeschi, E. (2018), "Review of control strategies for wave energy conversion systems and their validation: the wave-to-wire approach", *Renew. Sustain. Energ. Rev.*, **81**, 366-379. <https://doi.org/10.1016/j.rser.2017.06.074>.
- Wong, J. and Yi, J. (2018), "Design and study of spinning sea wave point absorber", *Project Report*. Universiti Sains Malaysia, Pusat Pengajian Kejuruteraan Mekanikal. (Submitted).
- Xu, L.H. and Li, Z.X. (2011), "Model predictive control strategies for protection of structures during earthquakes", *Struct. Eng. Mech.*, **40**(2), 233-243. <https://doi.org/10.12989/sem.2011.40.2.233>.
- Xuereb, A., Staines, C.S. and Staines, T. (2014). "Design of a linear electrical machine for a wave generation system in the maltese waters", *In book: Renewable Energy in the Service of Mankind* Vol I Chapter: 31. https://doi.org/10.1007/978-3-319-17777-9_31.
- Xu, W., Islam, M.R. and Zhu, J.G. (2020), "Guest editorial: Progress in electric machines, power converters and their Control for wave energy generation", *IET Elec. Power Appl.*, (14), 731-732. <https://doi.org/10.1049/iet-epa.2020.0306>.
- Yaramasu, V., Dekka, A., Durán, M.J., Kouro, S. and Wu, B. (2017), "PMSG-based wind energy conversion systems: survey on power converters and controls", *IET Elec. Power Appl.*, **11**, 956-968. <https://doi.org/10.1049/iet-epa.2016.0799>.
- Yaramasu, V. and Wu, B. (2017), "Model predictive control of wind energy conversion systems", Wiley-IEEE Press. <https://doi.org/10.1002/9781119082989>.
- Yemane, M. (2019), "Modelling and control of wave-to wire model of point absorber Wave Energy Converters (WECs)", *Master's thesis in Electric Power Engineering, Norwegian University of Science and Technology, Faculty of Engineering, Department of Electric Power Engineering*, June 2019.
- Ye, L. and Yu, Y.H. (2012), "A synthesis of numerical methods for modeling wave energy converter-point absorbers", *Renew. Sustain. Energ. Rev.*, **16**(6), 4352-4364. <https://doi.org/10.1016/j.rser.2011.11.008>.
- Zhang, A., Yaramasu, V., Rodriguez, J. and Zhang, Z. (2022), "Modulated predictive current control of back-to-back NPC converter in PMSG wind energy system with reduced computational burden", *Proceedings of the IEEE 7th Southern Power Electronics Conference (SPEC)*, Nadi, Fiji.

<https://doi.org/10.1109/SPEC55080.2022.10058345>.

PL